SIMULATING THE CHARACTERISTICS OF DROUGHTS IN SOUTHERN AFRICA

Master's dissertation

by

Eva Liliane Ujeneza

UJNEVA001

Presented towards the degree of Master's of Science in

Environmental and Geographical Science

University of Cape Town

February 2014

Supervisor: Dr. Babatunde J. Abiodun

Declaration

'I know the meaning of plagiarism and declare that all the work in the dissertation, save for that which is properly acknowledged, is my own.'

Signed by candidate

Signature Signature Removed

Name and Surname: Eva Liliane Ujeneza

Abstract

Drought is widely considered as one of the most devastating natural disasters in the world. In particular, drought is a big threat in Southern Africa because the economy of most of the population in the region is based on rain-fed agriculture. Previous studies have projected that global warming may enhance the frequency and intensity of droughts over Southern Africa in the future. However, the credibility of this projection depends on the ability of the global and regional climate models (GCMs and RCMs) in simulating the characteristics of drought. This thesis presents the characteristics of the Southern African droughts and evaluates the capability of global and regional climate models in simulating these characteristics.

The thesis used a multi-scaled standardized drought index (called standardized precipitation evapo-transpiration index, SPEI) in characterizing droughts at 3- and 12-month scales over Southern Africa. The spatial patterns of the droughts are identified using the principal component analysis (PCA) on the SPEI, while the temporal characteristics of the drought patterns are studied using wavelet analysis. The relationship between each drought pattern and global SSTs (and climate indices) is quantified using correlation analysis and wavelet coherence analysis. The study uses correlation analysis to quantify the capability of the models in simulating the drought patterns.

The PCA results show four main drought patterns that jointly explain about 50% of SPEI variance over Southern Africa. The drought patterns (hereafter PF1, PF2, PF3 and PF4) have their maximum loadings over the south-western part of Southern Africa (i.e. the common border of South Africa, Botswana and Namibia), Zimbabwe, Tanzania, and Angola, respectively. PF1, PF2 and PF4 are strongly correlated with sea-surface temperature (SST) over the South Atlantic, Tropical Pacific and Indian Oceans, while PF3 is strongly correlated with the SST over the Tropical Pacific, Atlantic and Indian Oceans. The drought patterns also

have significant coherence with some climate indices, but the strength, duration, and phase of the coherence vary with time.

The results show that GCMs and RCMs simulate the spatial patterns of drought better at 3-month scale than at 12-month scale. At a 3-month scale, 70% of the GCMs simulate all drought patterns with a high correlation coefficient ($r > 0.6$), but at a 12-month scale, none of the GCMs simulate all drought patterns with such a high correlation, although 60% of the GCMs reproduce at least three of the drought patterns with a high correlation coefficient ($r > 0.6$). Similarly, at 3-month scale, 75% of the RCMs simulate all drought patterns with a high correlation coefficient ($r > 0.6$), while at a 12-month scale, only 25% of the RCMs simulate all drought patterns with such a high correlation coefficient, but 90% of the RCMs reproduce at least three of the drought patterns with a high correlation coefficient ($r > 0.6$). The results of this study have applications in using the GCMs and RCMs for seasonal prediction of droughts, and for studying the impacts of global warming on droughts, in Southern African.

Acknowledgements

First of all, I praise God, the Almighty, for being my physical and moral strength through this work and for granting me the capability to successfully complete it. His unconditional love, blessings and protection are responsible for my achievements and successes in my life.

I would like to express my deepest gratitude to my supervisor, Dr Babatunde J. Abiodun for guiding my research, helping me to develop a strong background in atmospheric science and in climate modelling, and, most of all, for surrounding me with a friendly atmosphere for the past two years.

I would also like to express my gratitude to Philip Mukwenha, who was always keen to help with software installation and IT-related issues. Special thanks also go to Samantha L. Jenner for her help and patience during my first steps as a Ferret and Fortran programmer.

My gratitude goes to the University of Cape Town, the African Institute for Mathematical Sciences (AIMS), and the Applied Center for Climate and Earth Systems Science (ACCESS) for their financial support, and to the Climate Systems Analysis Group (CSAG) for providing both the financial and intellectual support. My research would not have been possible without the help of these institutions.

Finally, I am deeply grateful to my family, my sister and my mother, for their endless love, encouragement, and the moral and financial support, and for being where I could not be during work on the thesis. To my sweet daughter, for her patience and understanding, and for allowing me to be away; I am forever grateful. All your many sacrifices throughout the years are simply ineffable.

Dedication

To my late beloved father,

Ntaneza Donat

Table of Contents

List of Figures

List of Tables

List of Abbreviations

AAO - Antarctic Oscillation

CMIP5 - Coupled Model Intercomparison Project Phase 5

DKRZ - Deutsche Klimarechenzentrum

DWD - Deutscher Wetterdienst

ENSO – El Nino Southern Oscillation

GKSS - Helmholtz-Zentrum Geesthacht

IPCC – Intergovernmental Panel on Climate Change

SAM - Southern Annular Mode

SOI - Southern Oscillation Index

SPEI – Standardized Precipitation Evapo-Transpiration Index

Chapter I. Introduction

1.1 What Is Drought?

1.1.1 Drought definition

Drought has many definitions, depending on the field considered (i.e. social, economic, agricultural or environmental). For instance, a meteorologist might consider drought as a lack of precipitation, a hydrologist defines it as the period when the water available is less than the water demanded, while a farmer would consider drought as any period of low soil moisture (USGS, 2013). The lack of a unique definition for drought makes drought very hard to monitor. However, any drought is generally characterized by a deficiency of rainfall during an extended period of time. Besides precipitation amount, other meteorological factors play important roles in the occurrence and severity of droughts. For instance, high temperature may enhance evaporation that can reduce soil moisture. This may lower soil moisture and the water level in lakes and streams. Relative humidity, wind, pressure and potential evapotranspiration also influence occurrences and severity of droughts. Nevertheless, drought should not be confused with aridity or a heat wave. Drought differs from aridity and heat waves in many ways. While aridity, a permanent shortage of precipitation, is restricted to low rainfall areas (Wilhite, 1992), drought, a temporary shortage of water, can occur in any climatic zone (Ashok, 2010). On the other hand, heat waves, generally defined as extremely high temperature, only last for a few days (Bradfield, 2009), but drought is a lack of precipitation, not necessarily associated with high temperature, and can last for months or even years.

1.1.2 Types of droughts

Droughts can be categorized into four types: meteorological drought, hydrological drought, agricultural drought and socio-economic drought (AMS, 2004). The meteorological drought can be viewed as the general conception of drought. It occurs when there is a below normal

precipitation amount during an extended period of time (months, years, etc.) over a region. Lack of precipitation is the main cause of a meteorological drought.

A hydrological drought is characterized by a below normal average of water in a water resource management system (i.e. lakes, water reservoir). Hence, this type of drought can affects the hydrological system. Results from several studies show that, besides lack of precipitation, the geology of an area also plays a crucial role on the hydrological droughts (Vogel and Kroll, 1992; Zecharias and Brutsaert, 1988). The studies show that amount ground water reservoirs in an area depend on the physical structure and substance of the location area.

Agricultural drought occurs when there is a soil water deficiency. In this case, water available in the soil is not enough to support growth of crops and grasslands. Thus, primary consequences of agricultural drought are the damage of vegetation (crops, grass, and plants), though the severity of the damage depends on the specific characteristics of both the plants and the soil in addition to weather conditions (Mishra and Singh, 2010). Agricultural drought can also be enhanced by human activities like over-farming, deforestation, excessive irrigation (Mishra and Singh, 2010); erosion and poor water management (Dai, 2011).

Population growth, urban development, the establishment of new industries, tourism, and the development of energy and agricultural sectors also contribute to water scarcity. This kind of drought is called socio-economic drought. Mishra and Singh (2010) define socio-economic drought as one “that occurs when the demand for an economic good exceeds supply, as a result of weather-related shortfall in water supply”.

Different droughts have different temporal distributions. After a rain shortage, the time at which the impact of a drought will appear depends on the drought type. For instance, it takes a longer time to detect precipitation shortage in groundwater than in soil moisture. Therefore, different time scales are necessary to monitor different droughts. The time scale commonly used for drought monitoring ranges from weeks to 1 or 3 months for agricultural

droughts and from 12 to 24 months for hydrological droughts. The focus of the present study is on meteorological and agricultural droughts, which are generally measured at 3-, 6- and 12-month scales.

Drought indices are usually used to identify droughts and to classify them according to their intensity, severity, duration and geographical extension. The indices are helpful in extracting drought information from a variety of datasets. Nevertheless, the lack of a unique and universal drought definition has led to a variety of drought indices in the past century. For instance, the Standardized Runoff Index, Palmer Reclamation Drought Index, Palmer Hydrological Drought Index (Karl, 1986), Surface Water Supply Index (Shafer and Dezman, 1982; Doesken et al., 1991) and Palmer Drought Severity Index (PDSI; Palmer, 1965) are used to monitor hydrological droughts. The Vegetation Condition Index, Crop Moisture Index (Palmer, 1968) and Drought Monitor Index are used to monitor agricultural droughts. The Percent of Normal, Standardized Precipitation Index (McKee, 1993), and the Standardized Precipitation Evapo-transpiration Index (Vicente-Serrano et al., 2010) are for meteorological drought. Socio-economic droughts are more complex in concept, thus there are no indices for monitoring them yet.

1.1.3 Social and Economic Impacts of Droughts

Drought is widely considered to be one of the most devastating natural disasters in the world. Like any other natural hazard, droughts have negative impacts. However, droughts differ from other natural disasters, because they develop slowly and their impacts may be hardly detected initially, compared with for instance floods, earthquakes, volcanoes eruptions and hurricane. Furthermore, the impacts of drought can linger for a long time, even after the end of the drought (Mishra and Singh, 2010; Wilhite, 2000, Tannehill 1947). Between 1967 and 1991, droughts accounted for more than 33% of all human deaths that were attributed to natural disasters, and more than 1.2 billion people suffered from various drought impacts like shortage of water supply, destruction of crops and grasses, famine, and animal diseases and mortality (Obasi, 1994; Below et al., 2007).

Impacts of droughts (like reduction of hydro-electric power productivity and decrease of water in groundwater resources and reservoirs) can extend outside the drought region, owing to the interdependence between social groups and economic sectors (Wilhite et al., 2007). Another challenge is that droughts can occur in any climatic zone, in the tropical regions as well as in desert regions. Hence, the study of drought attracts scientists from several backgrounds (i.e. agriculture, environment, hydrology, meteorology, ecology, climatology, geology, and water management) worldwide. They all aim at a better understanding of drought in order to prevent and reduce its impact on the population and the environment.

1.1.4 Droughts in Southern Africa

Southern Africa is surrounded by two oceans. It lies in the middle of the southern tropics and experiences high climate variability. The region contains several political entities as South Africa, Zimbabwe, Malawi, Lesotho, Swaziland, Botswana and Namibia. Many parts of the region receive most of their annual rainfall during the austral summer (December to February), with the exception of a few areas along the south coast and the south-western region of South Africa (Ratna et al., 2012), the Western Cape, where the rainy season coincides with the austral winter (June to August), and East Africa, which receives its highest amount of precipitation during the long rainy season (mid-March to mid-June). In Southern Africa, the annual precipitation varies from 2 100 mm over the north-west region, to less than 10 mm over the Namibian desert, while the mean annual temperature varies from 9^{o}C to 31^{o}C, with the highest temperature along the north-east coast and north-west part of the region. Studies has shown that Southern African rainfall has a strong degree of inter-annual variability (Mason and Jury, 1997; Rouault and Richard, 2003), and its highest spatial-temporal variability is in the summer (Ratna et al., 2012). The inhomogeneous landscape and climate would contribute to the spatial distribution of droughts over the region.

Drought has a devastating impact on Southern Africa. According to Richard and Poccard, 1998, regions where the annual rainfall is between 300 and 500 mm are more vulnerable to droughts, and many parts of Southern Africa fall into this category (Mason and Jury, 1997;

Rouault and Richard, 2003). In 1972, Goldsberg classified the majority of Southern Africa as very vulnerable to drought, based on the difference between annual rainfall and potential evapo-transpiration. More recently, Clay (1995) has suggested that 60% of the region is (highly) vulnerable to drought. Therefore, the assessment of drought remains very important for authorities and water management planners of the Southern African region, especially in the countries where the socio-economy of people depends on agriculture (Jury, 2002; Washington and Downing, 1999). Since the economy of a large portion of Southern Africa's population is based on rain-fed agriculture, destruction of crops by drought could be very devastating, especially because drought is a reoccurring feature in the region (Rouault and Richard, 2005).

The increase in demand for water, owing to the actual growth of the population and expansion of agricultural and industrial activities, may also worsen drought impacts in the region. For instance, the droughts of 1991 and 1992 destroyed crops and caused huge agricultural and economic losses in Southern Africa (Calow et al., 2010). The droughts, which depleted groundwater reservoirs and reduced fresh water availability, forced many people to use water from unprotected sources. As a result, the people suffered from cholera, diarrhoea and dysentery (Calow et al., 2010). In the summer of 1992, more than 90% of small inland dams in the eastern part of Southern Africa dried, because the annual rainfall dropped 50% below normal (Jury and Mwafulirwa, 2002).

1.2 Problem Statement

There is a concern that the ongoing global warming may increase the severity of droughts in Southern Africa, because many studies have shown that drought severity increases with temperature (Dai et al., 2004; Dai, 2011; Sheffield and Wood, 2008; Washington and Preston, 2006; Vicente-Serrano et al., 2010). For instance, Dai et al. (2004) showed that, in the 1972–2004 period, the warming increased global dry areas by 20-38%. Dai (2011) found that the temperature increase of 1-3°C in 1950-2008 decreased the annual rainfall in most parts of Africa. The Intergovernmental Panel on Climate Change Fourth Assessment Report

(IPCC AR4; IPCC, 2007) projected a continuous increase in global mean surface air temperature over the 21st century owing to the increase in anthropogenic greenhouse gas concentration (Meehl et al., 2007), suggesting an increase in drought frequency, severity and spatial extension in future, especially in Southern Africa. Hence, the need to mitigate the impact of droughts in Southern Africa has led many studies to seek the underlying atmospheric dynamics that control rainfall variability over the region.

In Southern Africa, since many socioeconomic sectors (i.e. economic, agriculture, environment.) are affected by drought impacts, future projections of drought are a major tool for water and related activities' management and planning authorities. Therefore, to reduce the impact of droughts on human welfare and property over Southern Africa, there is a need to better our understanding of the characteristics of drought and the atmospheric dynamics that induce droughts over the region. This requires that the climate models, which are mathematical equations defined to simulate the climate system, are capable of simulating droughts over the region well. Since models perform differently in different regions, it is therefore important to evaluate the performance of climate models in replicating current and past droughts over Southern Africa. This will help to build confidence in simulated future drought, which is needed to evaluate the impact of global warming on potential future droughts.

1.3 Aims and Objectives

The present work aims to study the characteristics of Southern African droughts and evaluate the ability of climate models (GCM and RCMs) in simulating these characteristics. Thus the objectives are:

1. to study the characteristics (frequency, severity, spatial and temporal distribution) of Southern African droughts in past climate (1940 to 2009); and
2. to study how well global and regional climate models reproduce the Southern African droughts.

Answers to the above questions fill in current scientific gaps regarding the ability of regional downscaled and global climate models to replicate Southern African droughts. This study is the first of its kind in evaluating how reliable climate models' simulation of Southern African droughts is, using the SPEI. This study is first to use SPEI in evaluating how well GCMs simulate droughts in Southern Africa. We used SPEI because it is a standardised multiscale index that combines the influence rainfall and temperature in characterising drought. These properties make SPEI suitable for comparison over different domain and for identifying the impact of global warming on droughts (Vicente-Serrano et al., 2010).

1.4 Thesis Subdivision

Chapter 2 presents a summary of previous studies on droughts and evolution of the scientific opinion on the subject. Atmospheric and oceanic general circulations are considered as drought-inducing and drought-enhancing factors, and their relationship to Southern African drought is reviewed herein. The chapter also addresses the debate on the best drought index and presents our reasons for choosing SPEI as the drought monitoring tool for this study.

The standardized precipitation evapo-transpiration index (SPEI) is computed mainly from rainfall and temperature data. The methodology of how to compute the SPEI from monthly data is fully described in Chapter 3, together with an explanation of how to interpret the obtained outputs. Several analysis techniques are used in this work: the wavelet analysis, principal components analysis and many more. A short description of all the different analysis methods that are used in this study is also covered in this chapter.

The characteristics of past droughts in Southern Africa are presented in Chapter 4. The characteristics include the drought frequency, patterns, intensity, spatial coverage and the relationship with atmospheric tele-connections. Since the SPEI is a multi-scalar drought index, several time scales have been computed and observed in this study. Additionally, four areas were selected to allow for a deeper analysis. These areas are most vulnerable to droughts. The influence of general atmospheric and oceanic circulations are also studied

By comparing simulated historical drought with the observed, it is possible to evaluate the strength and weaknesses of climate models in replicating the droughts. Chapter 5 evaluates the ability of selected global climate models and regional climate models in replicating the Southern African droughts.

Lastly, Chapter 6 details our conclusions and the recommendations that follow from the study.

Chapter II: Literature Review

This chapter reviews findings from previous studies of droughts over Southern Africa. It reviews past works on drought indices, which are mathematical expressions that are used to determine droughts, and on the characteristics of past Southern African droughts. A review of the relationship between atmospheric tele-connections and Southern African droughts is presented. Finally, the chapter reviews the use and performance of climate models in simulating Southern African current and future climate and their contribution to the investigation of the global warming impacts on droughts.

2.1 Techniques for Evaluating Drought

2.1.1 Drought Monitoring

The Palmer Drought Severity Index (PDSI; Palmer, 1965), which uses precipitation, evapo-transpiration, soil moisture and temperature to determine moisture supply and demand, is the drought index that has been the most widely used (Mishra and Singh, 2010). Many modified versions of the PDSI have been defined, such as the Palmer Hydrological Drought Index (Karl, 1986), the modified PDSI (Heddinghaus and Sahol, 1991), the self-calibrated PDSI (Wells et al., 2004) and the Crop Moisture Index (Palmer, 1968). The main shortcoming of the PDSI is that its temporal scale ranges between 9 and 12 months only (Sivakumar et al., 2011; Vicente-Serrano et al., 2010).

The Standardized Precipitation Index (SPI), a multi-scale drought index developed by Mckee et al. (1993), is another popular drought index for detecting meteorological and agricultural drought at 3- and 6-month scale, as well as hydrological drought at 6-, 12-, 24- and 48-month scales (Hayes et al., 1999; Vicente-Serrano and López-Moreno, 2005; Vicente-Serrano et al., 2010). The SPI can detect wet and dry events occurring simultaneously at different time-scales. However, the main shortcoming of SPI is that it uses only one climate variable

(rainfall) for monitoring droughts (Sivakumar et al., 2011; Vicente-Serrano et al., 2011). It assumes rainfall has a stronger influence on droughts than other climate variables such as temperature, wind speed and direction, and potential evapo-transpiration; hence these variables are neglected. Before the early 1980s, this assumption was warranted, because precipitation seemed to be the dominant factor in terrestrial water changes; but, thereafter, other climate variables such as temperature, wind, and humidity have been shown to have equally, or even more, important than rainfall in influencing drought (Dai, 2011). For instance, if a given region received the same amount of rainfall during two different seasons under different temperatures, it was likely that the region would be drier during the warmer season owing to higher evaporation. However, to overcome the shortcomings of SPI, Vicente-Serrano et al. (2010) recently proposed a new drought index: the Standardized Precipitation Evapo-transpiration Index (SPEI), which depends on the potential evapo-transpiration (PET).

The Standardized Precipitation Evapo-transpiration Index (SPEI) is a modification of the SPI. Similarly to the PDSI, the SPEI also accounts for the effect of temperature variability in the monitoring of droughts, and like the SPI, it can be computed at different time scales. As a result, the Standardized Precipitation Evapo-transpiration Index can be used to detect the temporal and geographical extension of droughts, and this makes it a good tool for drought analysis and monitoring. Although SPEI has been used in several drought studies (Potop and Mozny, 2011; Vicente-Serrano et al., 2012; Vicente-Serrano et al., 2010), it has never been used to monitor Southern African droughts. Owing to its sensibility to temperature and its ability to account for the influence of global warming on droughts, SPEI is used for drought detection and analysis in the present study.

2.1.2 Decomposition Techniques

Many studies (i.e. Farge, 1992; Labat, 2005) have established the spectral analysis and the wavelet techniques as useful methods for identification of periodic modes (and their behaviour) in a given time series data. Both methods transform the time series data to

frequency domain. However, the methods differ in their transformation approaches and in their result presentations.

One of the shortcomings of the spectral analysis, which decomposes time series into a one-dimensional frequency signal, is that its Fourier basis functions are based on trigonometric functions that oscillate forever. This leads to the spread of any information along all the coefficients. On the other hand, the wavelet analysis, which decomposes any time series into a two-dimensional period-frequency space, allows for variability of all dominant processes in the time series.

Another superiority of the wavelet analysis over the spectral analysis is that it can be used to study different variability at different scales and does not need a stationary series (Ideião and Santos, 2005). Hence, wavelet analysis techniques have been widely applied worldwide. They have been used to uncover periodic cycles in rainfall data (Jury and Mwafulirwa, 2002; Jury and Enfield, 2002), to compare different drought indices (Ntale and Gan, 2003), to study inter-annual variability of SST (i.e. Rao et al., 2002), to examine the link between the variances of ENSO and monsoon (Torrence and Webster, 1999), and to investigate the influence of ENSO and IOD on summer rainfall in Zimbabwe (Manatsa and Matarira, 2009). On the other hand, Torrence and Webster (1999) used the wavelet transformation to analyse the timescales of the ENSO-Indian Monsoon system variability and the wavelet coherence to determine the link between the variance of ENSO and that of the monsoon. In the present study, we used the wavelet analysis to uncover periodic cycles in the PCA scores (i.e. time series) and to analyse the inter-annual variability of the region's main drought models. We used the wavelet coherence to study the variability of their relationship with large scale processes.

2.2 The Characteristics of Southern African Droughts

Several studies have investigated droughts over various parts of Southern Africa. For instance Manatsa and Matarira (2009) studied the change of Zimbabwean rainfall variability with ENSO and the IOD using the SPI as rainfall amount index and found no significant

changes in long-term rainfall trends, though a decreasing tendency was noticed during the 19th century. Various studies have shown that the region experienced severe droughts as a whole over large areas during the periods 1991/1992, 2002/2003 and 2003/2004 (Manatsa et al., 2012; Rouault and Richard, 2005; Unganai and Kogan, 1998). Some other studies investigated the changes in drought characteristics over the past century (Fauchereau et al., 2003; Richard et al., 2001). They all found that Southern Africa suffered from more widespread and intense droughts in the 1970s-1980s than in the 1950s-1960s; and some tried to determine future drought characteristics. For instance, Washington and Preston, 2006 suggested that it was likely that the vulnerability of the region to drought might rise in the future owing to climate change conditions, population growth, land degradation and deforestation, while Villholth et al., 2013 suggested that the region is at high risk of undergoing groundwater drought in case of a prolonged drought. Even though a lot has been done with respect to Southern African droughts, none of these previous studies have used the SPEI to describe the characteristics of Southern African droughts.

2.3 Impacts of Large Scale Climate Variability on Droughts

2.3.1 Impacts of Sea Surface Temperature

Since 1900s, the inter-annual variability of sea surface temperature (SST) is believed to be responsible for the variability of some climate variables. The dominant pattern of the variability of SST over the eastern equatorial Pacific Ocean is referred to as the El-Nino Southern Oscillation (ENSO; Douglas et al., 2007) and its pattern manifests as warmer SST associated with high air pressure. Another well known dominant pattern is the variability of the SST over the Indian Ocean, which is known as the Indian Ocean Dipole (also called Indian Ocean Zonal Mode; (Saji et al., 1999; Vinayachandran et al., 2009). The IOD is characterized by two phases of warming (cooling) of tropical SST over the eastern Indian Ocean associated with a change in the natural atmospheric conditions, namely a positive (negative) IOD phase.

By the end of the past century, there was a discussion about whether the IOD was a result of ENSO from the Pacific Ocean or the intrinsic variation of SST over the Indian Ocean. Behera

and Yamagata (2001) showed that there was a unique mechanism over the southern Indian Ocean by investigating the relation between the empirical orthogonal function (EOF) of the SST over the subtropical southern Indian Ocean. They found good a correlation between the first principle component (PC) times series and the SOI index but no continuous correlation was found between the second PC and ENSO and the Indian Ocean tropical dipole mode. Goddard and Graham (1999) showed that, in simulating rainfall over Southern Africa, the atmospheric response to Indian Ocean SSTs is more important than SSTs variability of the tropical Pacific Ocean. However, it has now been established that the IOD and ENSO present different patterns, though there is a strong link between Indian Ocean SST and ENSO (Washington and Preston, 2006).

A couple of studies have linked Southern African rainfall patterns with SSTs variability. For instance, Reason et al (2002) found a link between the winter rainfall over western South Africa and SST over the central South Atlantic Ocean. More recently, Mapande and Reason (2005) investigated the links between the variability of precipitation and SST patterns over western Tanzania and found that dry austral summers might be related to warm SST anomalies over the Indian Ocean. Furthermore, Washington and Preston (2006) used a simple statistical technique to investigate the impact of the Indian Ocean SST on extremely wet years in Southern Africa and found a connection between south-western Indian Ocean SST variability and enhanced poleward gradient with dry years.

Though a lot has been done to link SSTs variability with precipitation, less attention has been given to the relationship between droughts and SSTs variability over Southern Africa. Lamb and Peppler (1992) evaluated the influence of the tropical Atlantic surface atmospheric and the oceanic patterns on Sub-Saharan drought. They found that three of the four worse droughts (1972, 1977, 1983, and 1984) since 1940 were associated with positive (negative) SSTs in the southern (northern) part of the ocean. The 1983 severe drought differed from the others in that it was associated with positive SSTs over most of the tropical Atlantic. The present study assesses the relationship between global SSTs variability and drought patterns using the SPEI, which takes into account the temperature effects on drought.

2.3.2 Impacts of Atmospheric Tele-connection

Drought, as a rainfall dependent phenomenon, undergoes the influence of atmospheric tele-connections, which are defined as the linkage between climate anomalies of two widely separated regions. It is commonly understood that Southern Africa rainfall variability is mainly associated with ENSO (Lindesay et al., 1986; Matarira and Jury, 1997; Makarau and Jury, 1997; Fauchereau et al., 2003; Reason et al., 2000; Mason, 2001; Mishra, 2003; Philipon et al., 2011). Though, some studies suggest that there is no relationship between the Southern African winter rainfall and ENSO (Reason and Rouault, 2005; Blamey and Reason, 2007), some others specifically suggest that there might be a link between South African winter rainfall and ENSO (Reason et al., 2002; Philippon et al., 2011).

The relation of drought with atmospheric and oceanic circulations has been changing over the years. In fact, several studies have pointed out that the relationship between Southern African precipitation and ENSO has changed since the late 1960s (Richard et al., 2000; Fauchereau et al., 2003). They state that, before 1970, the summer rainfall was closely related to SSTs patterns over the south-eastern Indian Ocean and it became more correlated with SSTs anomaly patterns over the Pacific and Indian Oceans.

On the other hand, various studies pointed out that other general circulations may have a strong influence on Southern African rainfall as well. For instance the Indian Ocean Dipole/Zonal Mode is said to have a strong association with seasonal rainfall over Zimbabwe (Manatsa et al., 2008) and Southern African summer rainfall (Fauchereau et al., 2003; Manatsa and Matarira, 2009; Manatsa et al., 2012). In 2002, Jury and Mwafulirwa, using stratospheric zonal wind anomaly to investigate the relationship between Southern Africa rainfall and atmospheric tele-connections, suggested that the quasi-biennial oscillation (QBO) is closely associated with Malawi summer rainfall. Reason and Rouault (2005) found a link between western South African winter rainfall and the Antarctic Oscillation (AAO; also called Southern Annular Mode, SAM). Another study suggested that a large part of the spatio-temporal variability of subtropical Southern African rainfall might be directly related to tropical temperate troughs (TTT; Ratna et al., 2012).

Southern African droughts are believed to be ENSO dependant, because of the prevalence of dry events during warm ENSO episodes. For instance, Richard et al. (2002) found significant strong (weak) correlation between the southern oscillation index (SOI) and South African rainfall index (SARI) during the period mid 1930s-1990s and 1970s-1990s (mid 1930s-1960s). As mentioned earlier, these periods were classified as periods of intense drought for the Southern African region in the past century. Another study, Rouault and Richard (2005), suggested that ENSO might play a crucial role in defining Southern African drought and that most of the severe droughts that occurred in Southern Africa during the period 1901-2004 were associated with ENSO events. Some other studies go further and try to explain the absence of dry events during warm ENSO phases in Southern Africa. For instance, Nicholson et al. (2001) suggested that a weak atmospheric and oceanic coupling does not provoke drought over Botswana, but that, in that case, dry events tend to occur over Botswana when positive SSTs prevail in the Atlantic and Indian Ocean, and wet ones tend to occur when SSTs are predominantly negative in the Atlantic and negative or near normal, in the Indian Ocean.

2.4 Droughts Projections

2.4.1 Impacts of Global Warming on Droughts

The interaction between precipitation and temperature, and their contribution in drought occurrences, is quite complex. For instance, the increase in temperature is associated with a higher evaporation, which also depends on changes in precipitation frequency and intensity. Thus, although changes in future drought characteristics are linked to changes in future temperature and precipitation, this relationship is not straightforward (Sheffield and Wood, 2008). However, recent studies have shown the dependency of drought on temperature changes (Dai, 2011; Vicente-Serrano et al., 2011; Sheffield and Wood, 2008). Thus global warming, which has increased from 0.35°C (1910-1940) to 0.55°C (in 1970-2010); (Mishra and Singh, 2010), may alter the characteristics (frequency, severity and spatial coverage) of droughts in the future climate. Dai et al. (1998) suggested that the variation in drought spells from 1900-1995 could be explained by the ENSO shift towards more warm events (end of

1970s) and are consistent with the increase of greenhouse gases in the atmosphere. Dai et al. (2004) found that, from 1972 to 2004, surface warming contributed to an increase of the wet and dry areas in 20-38% of global land areas. More recently, Dai (2011) suggested that the temperature increase of 1-3°C over land areas during the period 1950-2008 and the precipitation amount decreased over most of Africa.

Many studies on climate model projections suggest that in future climates, frequency of droughts is likely to increase globally (Wetherald and Manabe, 2002), especially over Southern Africa (Haensler et al., 2011). The IPCC AR4 asserts that potential future temperature increases are likely to provoke changes in the hydrological cycle and enhance the occurrence of precipitation extremes. While investigating projected changes in drought occurrences on a global scale, Sheffield and Wood (2008) showed that drought duration is higher in Southern Africa, Australia, and North America, and at high latitudes, than elsewhere. According to Giorgi (2006), Southern Africa is one of the regions that will experience the highest changes in temperature and precipitation variability and mean, at a global scale in the future. All of the above studies have investigated drought variability owing to global warming at a global scale and none of them considered Southern African drought in particular. This might have caused them to miss some features, particular for the Southern African region. The present study investigates the matter by focussing on Southern African droughts.

2.4.2 Drought simulations with climate models

Climate models are mathematical equations that represent the climate system and that are defined following physical laws and principles, to reproduce observed characteristics of recent and past climate (Randall et al., 2007). Future projections of climate variables (including droughts) are usually made with Global Climate Models (GCMs) and Regional Climate Models (RCMs). These models use physical laws and parameters derived from observation to represent the global climate system (the atmosphere, the oceans, ice sheets and sea ice, and the land surface) by means of sophisticated computers. They are now the principal tools used by climate scientists to diagnose the causes of climate variability and to

make projections of future climate. Evaluation of climate models suggests that they perform less well in simulating precipitation than in simulating temperature, partly due to the weak relationship between rainfall changes and greenhouse gases. (Fauchereau et al., 2003). As a matter of fact, all models that were part of the IPCC AR4 reproduced the annual temperature reasonably well, giving a correlation of about 0.98 with observed data (Randall et al., 2007), but the models simulate precipitation poorly, especially the extremes in precipitation (Kiktev et al., 2003).

Several studies on drought projections are based on computation of drought indices using outputs from different climate models. Therefore, the prediction of future droughts is possible, as long as reliable future projections of rainfall are available (Mishra and Singh, 2011). There have been several attempts to analyse future drought projections on a global scale in the past. For instance, in Burke et al., (2006), the inter-annual variability of the first empirical orthogonal functions (EOFs) of the PDSI drought index computed from several simulations from HadCM3 is consistent with the one obtained from observations, though its spatial correlation coefficient over Southern Africa was only 0.31 (0.31 for Europe, 0.27 for Australia, 0.70 for USA and 0.51 globally). This raises the other challenge that climate models do not behave in the same way in different regions and, as such, need to be tested over different areas. More recently, Sheffield and Wood (2008) analysed changes in drought occurrences using soil moisture data obtained from eight AOGCMs that participated in IPCC AR4 under various emission scenarios (SRES A1B, B1 and A2). Although, they found that models replicated quite well the twentieth century drought characteristics, they also noticed that drought characteristics were overestimated at long term scales (12-months) and that models failed to simulate seasonal cycles for some part of Asia (China and Mongolia). More interestingly, their results show that the intensity and the spatial extent of short- (long-) term droughts become twice (three times) more common.

Since the GCM simulations are becoming more and more important tools for water management and planning, there is a need to investigate how well these models reproduce drought characteristics over different regions of the world. This knowledge may guide on the

reliability of the drought prediction from the models. Despite the volume of work on Southern African drought monitoring and modelling, no study has evaluated the ability of GCMs in reproducing the characteristics of Southern African droughts, especially using SPEI. This study evaluates the performance of GCMs and RCMs in simulating the drought patterns.

Chapter III: Methodology

3.1 Data

In this study, we consider Southern Africa as the region that extends from 0°S-37°S latitude to 0°E-45°E longitude. The topography of the region is shown in Fig 1. Data of different climate variables are used, like precipitation and temperature. We also use several types of atmospheric circulation indices. A large number of the data used was compiled by different internationally recognized institutions that provided them through their established websites. A short description of all variables data follows.

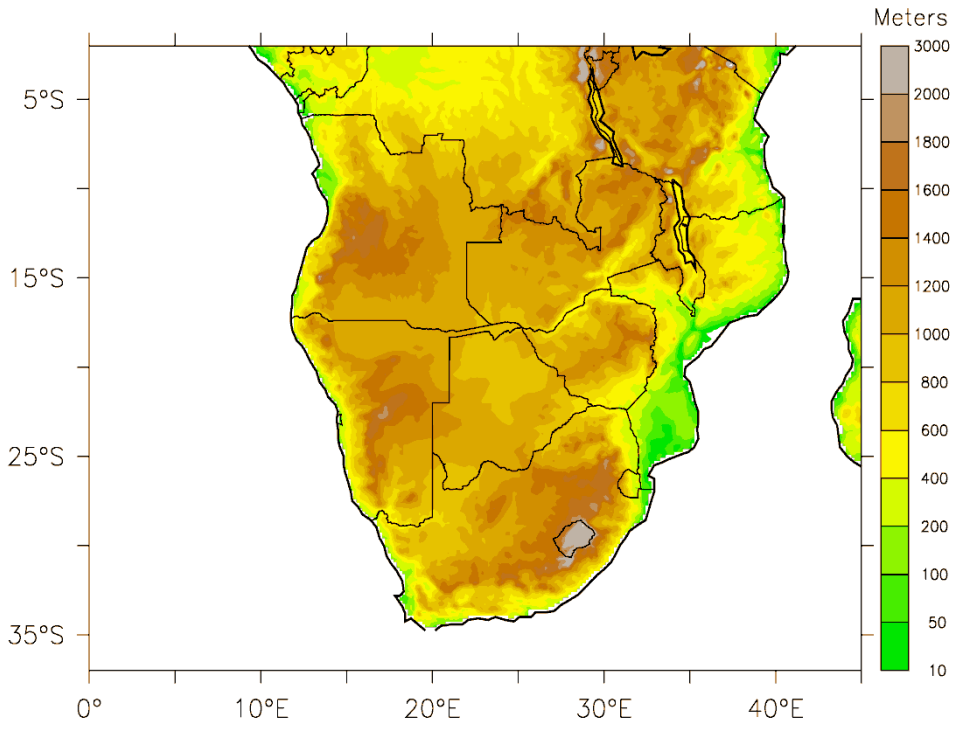

Figure 1: The study domain showing the topography in Southern Africa

3.1.1 Observed data

This study used the Climate Research Unit (CRU), University of Anglia, database of monthly gridded rainfall and temperature data that has 0.5°×0.5° degrees resolution and covers the

period of time 1901-2009. This precipitation database was obtained by merging several meteorological station data. Station sources are first checked for inhomogeneity using a technique similar to the GHCN automatic method of homogenization (Mitchell and Jones, 2005) and climate anomalies are then computed and interpolated. It has been shown that there are many inconsistences among observationally-based datasets over Africa, we used CRU dataset because it covers a longer period than any other observed datasets.

The study also used monthly sea surface temperature data from the global NOAA Extended Reconstructed SST dataset (Smith et al., 2008). This dataset has a high resolution of 0.5°×0.5° degrees and it covers the period from 1887 to 2009. The study used various climate indices to describe various atmospheric and oceanic circulations and the solar system (Table 1).

Table 1: Climate indices used in this study

Abbrevi-ation	Index name	Period	Data source
AAO	Antarctic Oscillation	1950-2009	Physical Sciences Division/ NOAA
IOD	Indian Ocean Dipole	1940-1997	Japan Agency for Marine-Earth Science and Technology
NAO	North Atlantic Oscillation	1940-2000	Climate Research Unit/ University of Anglia
QBO	Quasi-Biennial Oscillation	1948-2009	Physical Sciences Division/ NOAA
TNA	Tropical Northern Atlantic	1948-2009	Physical Sciences Division/ NOAA
TSA	Tropical Southern Atlantic	1948-2009	Physical Sciences Division/ NOAA
SOI	Southern Oscillation	1940-2009	Climate Research Unit/ University of Anglia
SSP	Sunspots Count	1940-2009	Solar Influences Data Analysis Center

3.1.2 Climate Models

We used the output from 10 GCMs. These GCMs are part of the Coupled Model Inter-comparison Project Phase 5 (CMIP5; Taylor et al., 2012), prepared for the Fifth IPCC

Assessment Report. Table 3 gives specifications on the surface level spatial and temporal resolutions for each GCM and indicates the developing institution. To avoid bias in the results owing to the differences between the spatial resolution and the time period covered by all GCMs, we first regridded them to a resolution similar to the CRU dataset and only considered the data for the period 1960-2002.

The study also used the output from eight RCMs from the Coordinated Regional Downscaling Experiment (CORDEX) project (Nikulin et al., 2012), which aims to provide regionally downscaled climate projections worldwide. CORDEX uses both statistical and dynamic techniques to obtain regional downscaled climate projections from Global Climate Models' outputs. All RCMs have the same horizontal grid resolution of 0.44°×0.44° and cover the period from 1989 to 2012. Information on the 8 RCMs is given in the Table 2, which indicates the institutions where each model has been developed.

Table 2: A description of RCM models used in this study

Model Name	Modelling Group	Country
CCLM	Potsdam Institute for Climate Impact Research (PIK)	Germany
CNRM	Centre National de Recherches Meteorologiques	France
CRCM5	Canadian Centre for Climate Modelling and Analysis	Canada
RACMO2	Royal Netherland Meteorological Institute (KNMI)	Netherland
RCA35	Rossby Centre regional atmospheric model – SMHI	Sweden
REMO	Max Planck Institute for Meteorology, DKRZ, DWD, GKSS	Europe
REGCM3	International Center for Theoretical Physics	Italy
WRF3	NCAR, NCEP, FSL, AFWA	Worldwide

Table 3: A description of all GCMs used in this study.

Model Name	Resolution	Period	Modelling Group	Country
GFDL-ESM2M	2.6 ˚ × 2.1˚	Jan 1956- Dec 2005	NOAA/Geographical Fluid Dynamics Laboratory	USA
MIROC-ESM-CHEM	2.8 ˚ × 2.8˚	Jan 1850- Dec 2005	Japan Agency for Marine-Earth Science and Technology, Atmospheric and Oceanic Research Institute, National Institute for Environmental studies	Japan
MIROC5	1.4 ˚ × 1.4 ˚	Jan 1860- Dec 2009	National Institute for Environmental studies, Atmospheric and Oceanic Research Institute, Japan Agency for Marine-Earth Science and Technology	Japan
CanESM2	2.8 ˚ × 2.7˚	Jan 1950- Dec 2005	Canadian Centre for Climate Modelling and Analysis	Canada
BNU-ESM	2.8 ˚ × 2.8˚	Jan 1950- Dec 2005	College of Global Change and Earth Systems Science, BNU	China
GFDL-ESM2G	2.6 ˚ × 2.1˚	Jan 1956- Dec 2005	NOAA/Geographical Fluid Dynamics Laboratory	USA
CNRM-CM5	1.4 ˚ × 1.4 ˚	Jan 1955- Dec 2005	Centre National de Recherches Meteorologiques	France
FGOALS-s2	2.8 ˚ × 1.66˚	Jan 1960- Dec 2005	LASG, Institute of Atmospheric, Chinese Academy of Science	China
HadGEM2-CC	1.9 ˚ × 1.25˚	Jan 1950- Dec 2005	Hadley Center for Climate Prediction and Research at the Meteorological Office	UK
Bcc_csm1	2.8 ˚ × 2.8˚	Jan 1850- Dec 2012	Beijing Climate Center (BCC), China Meteorological Administration	China

3.2 Estimation of Drought Characteristics

3.2.1 Drought Intensity: The Standardized Precipitation Evapo-Transpiration Index (SPEI)

We computed SPEI using the R software's library developed by Bergueria and Vicente-Serrano (2013) from precipitation and temperature data. A brief description of how the calculations are done follows. The first step is to compute the climatic water balance, with the difference D between precipitation and potential evapo-transpiration (PET), for each grid cell of the domain of interest. The evapo-transpiration can be thought of as the total amount of water that can be evaporated from an unlimited water-supplied surface. Given our region of interest, the assumption that all precipitation is rain is quite reasonable. Indeed, except for rare snow during some very cold winters in some specific regions and at high altitude, it is true.

Various studies have proven the superiority of the Penman-Monteith method (Shuttleworth, 1993), which incorporates radiation, humidity and wind speed data, over the method proposed by Thornthwaite (1948) that uses only temperature data and latitude, in computing the PET (Dai, 2011). However, in the present study, we used the Thornthwaite method. This choice was first motivated by a lack of several climate data (such as radiation, humidity and moisture) for the simulated data, and by the strong correlation (> 0.8) between results obtained for observation from both methods for most parts of Southern Africa (not shown).

The variable D is then be fitted with a log-logistic distribution, where the log-logistic distribution is the distribution of a random variable whose logarithm follows a logistic distribution. The probability density function f(x) of a log-logistic distribution is

$$f(x) = \frac{\beta}{\alpha}\left(\frac{x-\gamma}{\alpha}\right)^{\beta-1}\left[1+\left(\frac{x-\gamma}{\alpha}\right)^{\beta}\right]^{-2},$$

with $\gamma \leq x < \infty$, $\alpha < 0, \beta < 0$ and $\gamma < 0$; where α is the scale parameter, β is the shape parameter and γ the location parameter.

The parameters of a log-logistic distribution can be estimated using various methods like the maximum likelihood method, the conventional moments or L-moments. Vicente-Serrano et al. (2010) used L-moments to estimate log-logistics parameters. According to Hosking (1990), L-moments can give more accurate estimates than the maximum likelihood method and, owing to their linearity, L-moments are less sensitive to outlying data than conventional moments. The probability-weighted moments are first computed from the frequency estimator F_i of the computed variable D_i as follows:

$$w_s = \frac{1}{N}\sum_{i=1}^{N}(1 - F_i)^s D_i ,$$

where N is the number of observations in the variable D and the frequency estimator computed as $F_i = \frac{i - 0.35}{N}$. L-moments λ_i are then obtained using the formulae:

$$\lambda_1 = w_0 ,$$

$$\lambda_2 = w_0 - 2 w_1 ,$$

$$\lambda_3 = w_0 - 6 w_1 + 6 w_2 ,$$

$$\lambda_4 = w_0 - 12 w_1 + 30 w_2 - 20 w_3 .$$

Although, in their work, Vicente-Serrano et al. (2010) did not clearly explain how log-logistic estimate parameters are obtained, they can be easily computed as

$$\beta = \frac{\lambda_3}{\lambda_2}$$

$$\gamma = \lambda_1 - \frac{\lambda_2^2}{\lambda_3}$$

$$\alpha = \lambda_2 \frac{\sin(\pi\beta)}{\pi\beta^2}$$

where α, β and γ are the estimated scale, shape and location shape parameters respectively (Fitzgerald, 2005). After calculating the estimates, the cumulative distribution of the data is therefore calculated using the formula below:

$$G(x) = \left(\frac{x - \gamma}{\alpha}\right)^{\beta}\left[1 + \left(\frac{x - \gamma}{\alpha}\right)^{\beta}\right].$$

A transformation is then applied to obtain a standard normal variable from the cumulative probability of the variable *D*. Different methods can be used for this purpose. In their work, Vicente-Serrano et al. (2010) used the Abramowitz and Stegun (1965) approximation. Given the cumulative probably *G(x)* of a sample of data, the standard normal variable Z is:

$$Z = U - \frac{c_0 + c_1 U + c_2 U^2}{1 + d_1 U + d_2 U^2 + d_3 U^3},$$

where $U = \sqrt{2\ln(H(x))}$ for $0 < H(x) \leq 0.5$ with *H(x) = 1 – G(x)* being the probability of exceeding a *D* value. In the case $H(x) > 0.5$, then H(x) = G(x) is used and the sign of *Z* is reversed, then the variable *U* is $U = \sqrt{2\ln(1 - H(x))}$. The constants are *c0 = 2.515517; c1 = 0.802853; c2 = 0.010328; d1 = 1.432788; d2 = 0.189269 and d3 = 0.001308.*

The SPEI is the obtained variable *Z* and in general it ranges between -3 and 3. Those values help determine the intensity of the drought. The more negative the SPEI, the more severe the drought.

3.2.2 Drought Frequency

Drought frequency means the number of times dry events occurred. We used SPEI ≤ -1.0 to designate drought and defined drought frequency as the number of months with a low SPEI. Note that the drought frequency as defined in this work would attribute a frequency of five to a drought that lasted five consecutive months rather than a frequency of one.

3.3.3 Drought Patterns: Principal Component Analysis

The study used the principal component analysis (PCA) on the SPEI data to obtain the spatial-temporal characteristics of the SPEI. PCA, which reduces the dimensionality of a dataset and uncovers hidden structures in the dataset, has been used in many studies to extract useful information from huge or confusing datasets (i.e. Giannini et al., 2008; Manatsa et al., 2012; Richard et al., 2001). PCA is mainly used to reduce the dimension of the data and to uncover hidden structures, if any. The PCA being a non-parametric method, it can be used with data following any distribution, which makes it a valuable tool. In the climate field, PCA is mostly used in order to discover the different processes that control the climate variability, like rainfall (Richard et al., 2000; Richard et al., 2001). In the present we use PCA to identify processes that control the spatial and temporal patterns of Southern African drought.

The method consists of first computing the covariance matrix of the standardized normalized variables (the correlation matrix can also be used instead). When the variables have different units, the use of the covariance matrix allows the variable of higher values to weigh more. Given a set of n variables, with a time dimension of N, they can be represented by X_n^N. Their matrix of covariance M is defined as follow:

$$M = \begin{pmatrix} cov\left(X_1^N, X_1^N\right) & cov\left(X_1^N, X_n^N\right) \\ cov\left(X_n^N, X_1^N\right) & cov\left(X_n^N, X_n^N\right) \end{pmatrix}$$

where

$$cov(X_i, X_j) = \frac{\sum_{i=1,j=1}^{n} (X_i - X_i)(X_j - X_j)}{N - 1}.$$

The following step is to compute the eigenvectors and eigenvalues of the covariance matrix, and then the eigenvectors are ordered following the values of their associated eigenvalues. The eigenvectors are therefore ordered according to the values of their associated eigenvalues, and the first principal factor is the eigenvector that has the highest value and, hence, represents the mode with highest variance in the dataset. The first principal factor represents the strongest relationship between the variables' dimensions.

Here, PCA was used to identify the spatial coherence (modes or patterns) in temporal variability of the SPEI. Dimensions of different variables are replaced by the evolution of one variable, the SPEI, over time, over different grid cells. The first principal factor represents the process that has more control on the SPEI spatial and temporal patterns. PCA was applied separately on the CRU and GCM SPEI. For each dataset, the first four principal factors of the PCA were retained and discussed as the most significant modes in the dataset.

3.3 Analysis Methods

3.3.1 Mann Kendall Trend test

The Mann Kendall trend estimator is a non-parametric trend that allows the determination of a linear trend in a given time series. The probability of the presence of an upward or downward trend is evaluated and tested. Being non-parametric, the Mann Kendall trend test can be applied to any statistically distributed data and has been used in different climatological studies. To apply the technique, the MK-statistic S is first calculated, together with its associated probability. The variable S is originally set as zero. A comparison of any data point with its previous one is done, starting with the second data point of the evaluated variable. For any data point whose value is greater than the value of the previous point, the

MK-statistic S value is increased by one. One is subtracted from S , for any data point whose value is lower than the value of the previous one.

$$S = \sum_{j=1}^{n-1} \sum_{i=j+1}^{n} sign\left(x_i - x_j\right)$$

where

$$sign\left(x_i - x_j\right) = \begin{cases} 1, \text{ if } x_i - x_j > 0 \\ 0, \text{ if } x_i - x_j = 0 \\ 1, \text{ if } x_i - x_j < 0 \end{cases}$$

The number of data points n in the evaluated variable determines the variance of the MK-statistic, which also depend on the number of data points t that are in a tied group g . It is calculated as shown below.

$$Var(S) = \frac{1}{18} \left(n(n-1)(2n+5) \sum_{p=1}^{g} t_p \left(t_p - 1\right)\left(2t_p + 5\right) \right)$$

where t_p is the number of similar data points that are in the p^{th} tied group. The probability associated with the MK-statistic is obtained by calculating the standard normalized test statistic of the normalized variable Z :

$$f(Z) = \frac{1}{\sqrt{2\pi}} \exp\left(\frac{z^2}{2} \right)$$

Where, the normalized variable

$$Z = \begin{cases} \frac{s\text{-}1}{\sigma}, S > 0 \\ 0, \ S = 0 \\ \frac{s+1}{\sigma}, S < 0 \end{cases}$$

Two hypotheses are then defined to make the trend test:

$$\begin{cases} H_0 \text{ there is no trend} \\ H_1 \text{ there is a trend} \end{cases}$$

The two hypotheses are associated with a probability called "level of significance". This level of significance represents the probability of rejecting the null hypotheses H_0 when it is true, and it is generally taken as 5% or 1%. If the probability of the test statistic $f(Z)$ is less than the chosen level of significance, the time series is concluded to not have a trend and the null hypothesis is said to be true. When the probability of the test statistic $f(Z)$ is greater than the level of significance, the null hypothesis is rejected and the times series has a trend. The sign of the normalized test statistic determines the upward or downward characteristic of the trend. A positive normalized test statistic indicates a positive or increasing trend, while a negative one indicates a decreasing trend.

3.3.2 Wavelet Analysis

Wavelet analysis is a technique that transforms a given signal into a two-dimensional period-frequency space. Applied on climate variables, it allows the identification of the various periodic processes that have influenced them at different periods of time. In the present work, we used the R library "biwavelet" (Gouhier and Grinsted, 2013) for all wavelet analysis calculations. A short description of the mathematical aspect of wavelet analysis is given below.

The wavelet technique is based on the logic of Fourier analysis, but it addresses the later shortcomings by using different scales to analyse different frequencies, contrary to the

Fourier analysis that uses the same scale for all frequencies. As a result, the wavelet transformation can use good frequency resolution and poor time resolution at low frequencies, as well as good time resolution and poor frequency resolution at high frequencies.

The wavelet analysis uses analysing functions, called wavelet basis functions; they are defined in space and are independent of the scale parameter. There are several wavelet basis functions, namely Morlet, Paul and Derivative of Gaussian (DOG) to only cite a few. The mathematical expression of these wavelet basis functions and some of their properties are presented in Annexe 1 (more examples and details can be found in Farge, 1992). In the present work we used the Morlet wavelet function

$$\psi_0(\eta) = \pi^{1/4} e^{i\omega_0 \eta} e^{-\eta^2/2},$$

which has a zero mean and is defined in frequency (ω_0) and time space (η). The choice of this function was motivated by the fact that it is a complex function, in contrast to DOG, which allows the determination of oscillatory behaviour (Torrence and Compo, 1998).

One of the wavelet analysis techniques consists of approximating the continuous wavelet transformation of a time series x_n by computing its convolution W_n with a scaled version of a wavelet basis functions several times:

$$W_n(s) = \sum_{n'=0}^{N-1} x_{n'} \Psi^* \left[\frac{(n'-n)\delta t}{s} \right],$$

where ψ is the complex conjugation of the wavelet basis function, *n* is the number of time point and s is the wavelet scale that serves to dilate or contract the analysing wavelet function.

Though it is possible to do the convolution for n times (with $n < N$) for each scale by taking only every n point, it is more efficiently to make use of the convolution theorem and

compute simultaneously N convolutions using a Discrete Fourier Transform (DFT) of the time series. Given the time series x_k of length N, the DFT of the variable is:

$$F\{x_k\} = x_k = \sum_{n=0}^{N\ 1} x_n \exp\left(\frac{2\pi i k n}{N}\right)$$

where $k = 0,1,2,...,N\ \ 1$ represents the frequency index. From the convolution theorem, the wavelet transformation is then:

$$W_n(s) = \sum_{k=0}^{N\text{-}1} x_n \psi^*(s\omega_k) e^{-i\omega_k nt\delta}$$

where $\psi(s\omega)$ is the Fourier transformation of $\psi(t/s)$, in the continuous domain and ω_k the angular frequency that could be represented using a piecewise function as below

$$\omega_k = \begin{cases} \dfrac{2\mathrm{k}\pi}{Nt\delta}, \text{for } k \le \dfrac{N}{2} \\ -\dfrac{2k\pi}{Nt\delta}, \text{for } k > \dfrac{N}{2} \end{cases}$$

One thing to consider while computing these wavelet transformations is to make sure that they could be comparable among them at all scales. To ensure that, the wavelet function is normalized at each scale in such a way that it will have unit energy (Torrence and Compo, 1998). Then at each scale s, we obtain

$$\sum_{k=0}^{N-1} |\psi(s\omega_k)|^2 = N$$

The wavelet power spectrum could then be defined as $|W_n(s)|^2$ and the amplitude as $|W_n(s)|$ at each scale, as Torrence and Compo (1998) suggested. The present work uses the unbiased definition of the wavelet power as $2^s \times |W_n(s)|^2$, as suggested by Liu et al. (2007). More details on the calculation of the wavelet transformation and the wavelet power spectrum can be found in Torrence and Combo (1998) and Liu et al. (2007).

Another wavelet technique is to compute the wavelet coherence. The wavelet coherence identifies simultaneously the time intervals and the frequency bands, where two time-series are correlated. It is obtained by first computing the wavelet transformations $W_n^X(s)$ and $W_n^Y(s)$ of both time series X and Y respectively, followed by their cross-wavelet spectrum

$$W_n^{XY}(s) = W_n^X(s) W_n^{Y*}(s)$$

where * means the complex conjugate. The wavelet coherence $R_n(s)$ is then defined as

$$R_n^2(s) = \frac{\left| \left\langle s^{-1} W_n^{XY}(s) \right\rangle \right|}{\left\langle s^{-1} \left| W_n^Y(s) \right|^{-2} \right\rangle \left\langle s^{-1} \left| W_n^X(s) \right|^{-2} \right\rangle}$$

where $| \, |$ is the absolute value and $\langle \, \rangle$ means smoothing in both time and scale. The smoothing is done by applying a convolution (weighted running average) over both the time and scale. More details on this can be found in Torrence and Webster (1999).

3.4 Droughts Analysis

This section presents in detail how the present work uses the different mathematical tools and analysis techniques to address the research questions explained in Chapter one.

3.4.1 Determine characteristics of Southern African droughts during the period 1940-2002

The present study evaluates the different characteristics of Southern African droughts, like their frequency, intensity, and temporal and geographical extensions, for the period from 1940 to 2009. The Standardized Precipitation Evapo-transpiration Index is first computed at 3- and 12-month scales from observed rainfall and temperature variables data, in order to determine past drought characteristics over each grid of the defined domain. The study then applied a principal component analysis (PCA) on the SPEI in order to determine the droughts' patterns over the region. For both SPEI datasets, only the first four principal factors of the PCA, which show the most influence on the data, were retained. Four sub-

regions were derived from the SPEI loadings as the most linked to each mode respectively. The averaged SPEI over each sub-region was then evaluated to determine the severity of the droughts following their associated SPEI: the lower the SPEI; the more severe the drought.

The study also determines the drought frequency for each sub-region per decade and evaluates its variability over the years. We determine the beginning and the end of any severe drought by investigating the corresponding SPEI, at the lowest time scale. The geographical extension of each dry event is identified, using SPEI maps of Southern Africa. Furthermore, the study determined the drought trend at each location of the region of interest using linear regression on SPEI calculated data. The significance of the trend was evaluated with the Mann-Kendall trend test. This enabled us to check the existence of a linear positive or negative trend, which indicates an increase or decrease in droughts respectively.

3.4.2 Investigate the link between atmospheric-oceanic circulations and Southern African droughts

We apply two different methods, Principal Components Analysis (PCA) and wavelet analysis, on the SPEI calculated time series in order to investigate processes that have an influence on droughts. For the PCA, we try to identify the different principal factors (PFs), with atmospheric-oceanic circulations, the solar cycle or other processes, by computing the correlation between climate variable indices and the scores of the PFs. The correlation between the scores of all principal factors and the global sea surface temperature was also evaluated in order to enable a first identification of the processes that induce droughts in the region.

On the other hand, we apply the wavelet analysis to analyse the variability of the influence of the drought modes over time. The use of the continuous wavelet transformation allows the identification of the periodic signals in any given time series and enables the evaluation of their potential similarities with the SPEI power spectrum over time. Since the wavelet power spectrum gives information about the different processes that control a given

variable over time, we computed it for each PFs' score. The cyclic phenomenon with the highest amplitude at any particular time is the one that influences the most the variable for that period. We also computed the wavelet coherence between each score and some climate variable in order to identify the variability of their relationship. This enables us to clarify the variability of the influence of different phenomena over Southern African droughts.

3.4.3 Evaluate the ability of the climate models in capturing droughts over Southern Africa

Testing the ability of models in simulating present and past climate is very important in order to determine how reliable model simulations are. In this work, we mainly evaluate the ability of models to reproduce spatial and temporal features of drought patterns rather than drought itself. First, we compute the SPEI at each grid cell and for each model. Then a PCA analysis is applied to the SPEI computed from each model's output and only the first four PFs are retained. We then evaluated the models by comparing each simulated score (only from RCMs) and loadings (from both GCMs & RCMs) with those of the observed by using temporal correlation and simple matching respectively. The more similar to those of the observed a model's loadings are, the better the model's behaviour and the higher the correlation between a model's score and that of the observed, thus the better the model's performance.

Chapter IV: Characteristics of Past Droughts in Southern Africa

This chapter discusses characteristics of past droughts in Southern Africa. The standardized precipitation evapo-transpiration index of the entire domain is analysed using principal components analysis in order to investigate their link with tele-connections. Order characteristics like frequency and intensity are presented for four chosen sub-regions with highest variance of SPEI.

4.1 Drought Characteristics

4.1.1 The Spatial structure of Southern African droughts

Figures 2a - d and 3a - d present the PCA loadings of the first principal factors and indicate the dominant patterns in the 3- and 12-month scale SPEI over Southern Africa. These patterns (hereafter, namely PF1, PF2, PF3, and PF4) jointly explain about 45% (50%) of the total variance in the 3-month (12-month) SPEI dataset. PF1 explains 19.1% of the SPEI variance at 3-month scale and 19.1% at 12-month scale. It shows its highest loadings (0.8) over the south-west area of Southern Africa (i.e. over the border of South Africa, Botswana and Namibia; hereafter Area 1) which then diminish regularly towards the equator (Fig 2-3a). PF2 explains 12.2% of the variance of the 3-month SPEI and 9.47% of the 12-month SPEI. It shows loadings with opposite signs, with peaks at 0.8 and -0.8 over the eastern (over Zimbabwe; named Area 2) and over the south-western (over Western Cape) regions, respectively (Fig 2-3b). This suggests that whenever PF2 imposes dry conditions over Zimbabwe, it imposes dry conditions over the Western Cape, and vice-versa. PF3 explains about 10.5% and 11.1% of the 3- and 12-month SPEI variance. PF3 shows a dipole pattern in its loadings (Fig 2-3c): a positive peak (about 0.8) over Tanzania (Area 3) and a negative peak (about -0.3) over the south-east of South Africa.

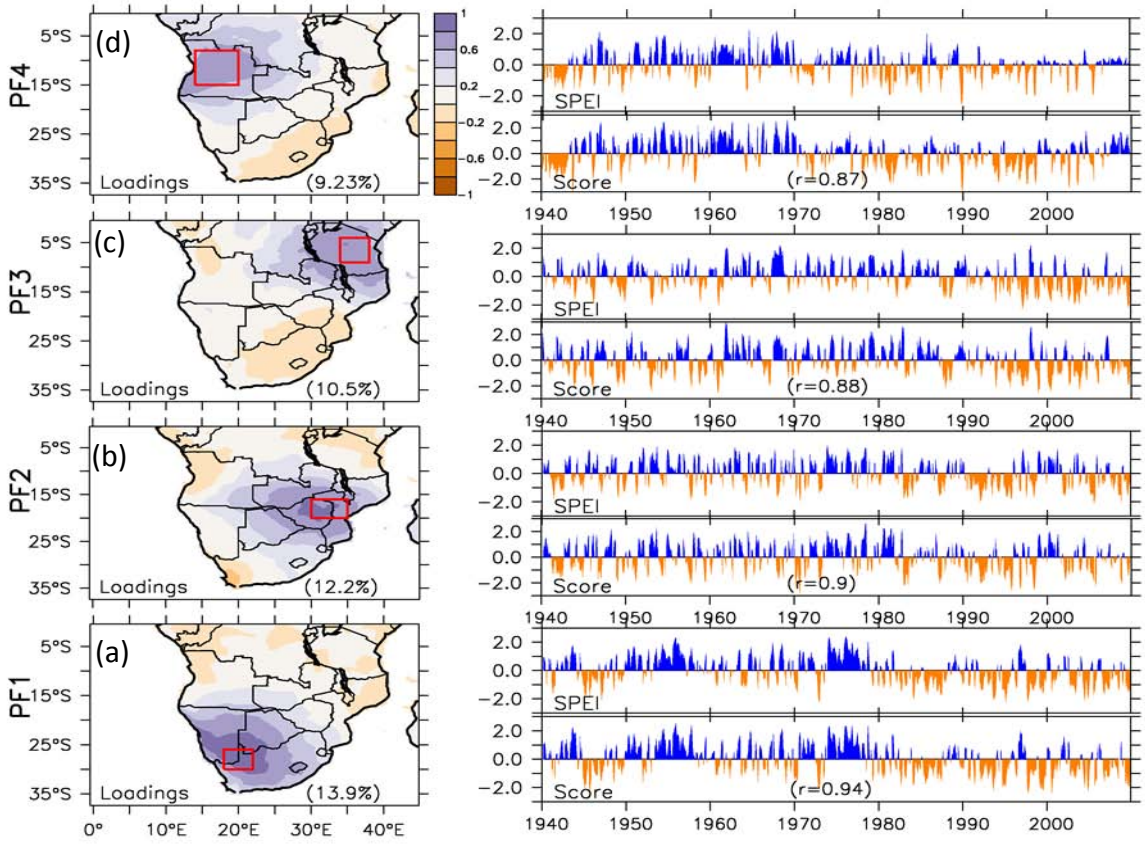

Figure 2: The spatial-temporal variability of 3-m SPEI over Southern Africa. The left panels show the PCA loadings of the SPEI and the percentage of variance explained by each principal factor (PF). The right panels show the corresponding PF score, the SPEI series averaged over the area in the red box in the left panel, and the correlation (r) between the PF score and the SPEI series.

The PF4, which explains 9.23% (10.3) of the 3-month (12-month) scale SPEI variance (Fig 2-3 d), controls the dry and wet conditions over Angola (Area 4) and over the south-eastern part of Southern Africa, where it shows positive loadings (about 0.7) and negative loadings (about -0.3) respectively. The similarities between the patterns at 3-month and 12-month scale suggest that processes that seem to drive short-term droughts in Southern Africa are the same as those that induce long-term droughts.

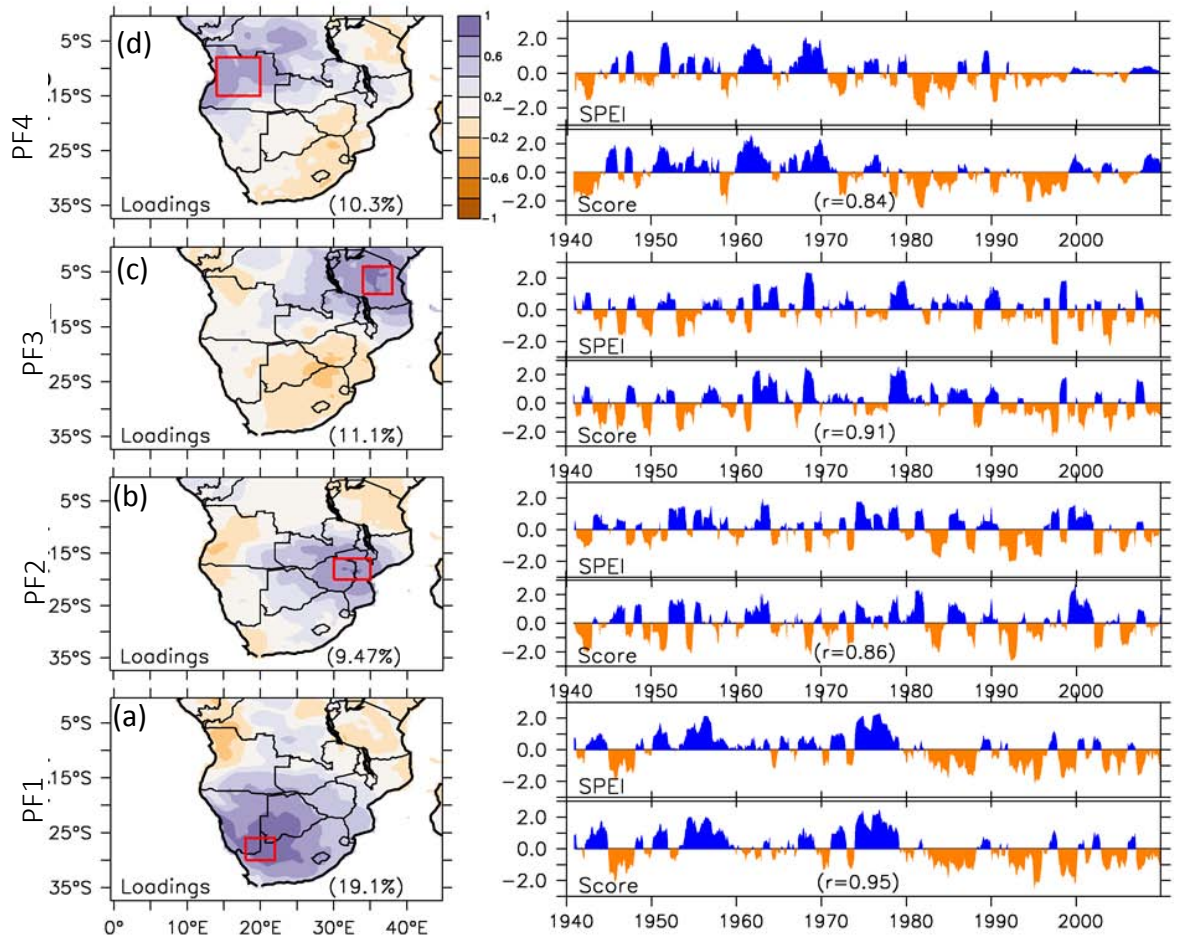

Figure 3: The left panels show the PCA loadings of the 12 months SPEI and the percentage of variance explained by each principal factor (PF). The right panels show the corresponding PF score, the SPEI series averaged over the red box in the left panel, and the correlation (r) between the PF score and the SPEI series.

4.1.2 The Temporal structure of Southern African droughts

In general, all time-series of SPEI over the selected area show high correlations with their corresponding mode ($r > 0.8$), at both 3- and 12-month scales. This means that each mode has a close relationship with more than 64 % of all droughts that occur in its corresponding area. Note that all these areas were chosen as those where the influence of the drought modes were the strongest and, as such, lesser correlation are to be expected if different regions were considered.

In particular, the PF1 score shows a high correlation (r = 0.93) with the time series of the 3-month scale SPEI over area 1. The SPEI evolution (Fig 2a) shows that the area experienced severe droughts during the periods 1984, 1987, 1992-1993, 1994-1995, 1997 and 2004-2005; the more severe and longer drought in the period 1945-1950, while the most severe drought (SPEI ≈ -2.3) occurred in 1972. Moreover, a deeper observation reveals that the three last decades of the period of study (1980s to 2000s) were dominated by the occurrence of dry events while, during the three previous ones (1950s to 1970s), wet events were mainly dominating. This implies that droughts have become more intense and severe than before the beginning of the 1980s. These results are consistent with findings from previous studies that found an increase in drought intensity (i.e. (Holm and Morgan, 1985; Manatsa et al., 2012; Rouault and Richard, 2005; Unganai and Kogan, 1998).

The score of PF2 shows a high correlation (r =0.9) with the time series of the 3-month scale SPEI over Zimbabwe (Fig 2b). The SPEI time series indicates that Zimbabwe experienced severe droughts in 1983, 1987, 1992, 1995, 2002, 2005 and 2008, with the most intense drought in 2005. Differently from the previous region, the country seems to have experienced several droughts of similar intensity throughout the years, without the increase of the SPEI intensity. According to Fig 2b, the main dry events occurred in the decades of the 1940s 1980s, 1990s and 2000s over Zimbabwe.

The correlation between the score of PF3 and the time series of the 3-month SPEI over Tanzania is also very high (R=0.88, Fig 2c). The time series indicates that Tanzania experienced severe droughts in 1953, 1961, 1997, 2002, 2003 and 2009, with the most severe drought occurring in 1997. This is in line with results from previous studies (e.g. Paavola (2008)) that classified 1997 and 2003 as drought years for Tanzania, defining drought as any monthly rainfall that is less than a third of the long-term mean. Here also we observe an increase in drought intensity in the averaged SPEI, but, unlike for PF1 and PF2, the wet and dry events are more evenly distributed over the whole study period. Furthermore, the 1970s was the wettest decade of the study periods for Tanzania.

The score of PF4 shows a high correlation (R=0.85) with the SPEI time series over Angola (Fig 2d). The time series indicates that Angola encountered its more severe and longer drought in 1976, 1981, 1989/1990, 1998 and 2005, with the most severe drought (SPEI = -2.455) in 1989. Area 4 SPEI evolution is quite similar to that of Area 1; however, unlike it, it has low drought intensity and shows near normal conditions for the last decade (2000-2009).

The correlation between each 12-month SPEI time series and its corresponding score is high: 0.95, 0.86, 0.91 and 0.84 for PF1, PF2, PF3 and PF4 respectively (Fig 3a-d). The evolution of averaged SPEI for all four processes is similar to that in Fig 2, except some small differences, mainly about the year each area experienced its most extreme drought. The most severe drought that happened in the area covering the common border between South Africa, Namibia and Botswana, occurred in 1995, with a SPEI index of about -2.3. Tanzania experienced its most severe annual drought in 1997 (SPEI ≈ -2.261), Angola in 1981 (SPEI ≈ -2.225) and Zimbabwe in 1992 (SPEI ≈-1.904). One can explain the discordance between the year of extreme drought at 3-month scale and the one obtained at 12, exception made of the PF3 case, with the possibility of having only one extremely dry season (3-month scale drought) in a considered 12 month periods. The SPEI being an index that depends on past observations, the above scenarios might give an SPEI value (between -1 and 1 in our case) that indicates quite normal conditions (neither wet nor dry) at 12 month scale for that particular year.

In general, the four PFs induce droughts that present similar patterns, except for a few differences. All areas present an increase in the intensity and duration of drought at both short and long time-scales from the 1980s until the mid-2000s. The exception is Area 4. The period from the 1970s to the 1990s was the driest for this area, at both 3- and 12-month scales. These results are consistent with findings from previous studies. For instance Richard et al. (2001) showed that Southern Africa has experienced more widespread and more intense droughts in the 1970s -1980s than in the 1950s-1960s. Moreover, other studies suggested that there have been a global increase in drought intensity and spatial expansion since the 1970s (Manatsa et al., 2008; Lamb, 1996) that might be owing to a stronger

relationship between Southern African rainfall and ENSO (Rouault and Richard, 2005). Another discrepancy is the drought evolution over Area 4, which seems to follow a completely different pattern: while others show a general increase in drought frequency and intensity in the 1990s and the 2000s at all time scales, Area 4 surprises with the absence of drought at 12-month scale over the last decades and at 3-month scale at the end of the 2000s.

The trend analysis, applied on each SPEI time series, shows that there is a slight significant downward trend over all four areas (see Table 4). This means that, as the time goes by, the intensity and/or the number of dry events are increasing in these areas.

Table 4: The trend of the SPEI for all areas.

3-month (12-months) SPEI				
	Area1	Area2	Area3	Area4
normalized test statistic	-0.099 (-0.0863)	-0.201 (-0.267)	-0.155 (-0.113)	-0.145 (-0.164)
p-value (2 sided)	1×10^{-5} (0.0001)	2×10^{-16} $2 \times 10^{-16})$	2×10^{-11} (8×10^{-7})	3×10^{-10} (1×10^{-12})

4.1.3 Drought Frequency

Figure 4 indicates that in general there has been a gradual increase in the drought frequency for all the drought patterns at both 3- and 12-month scales, from 1970 to the 1990s, except for Area 4.

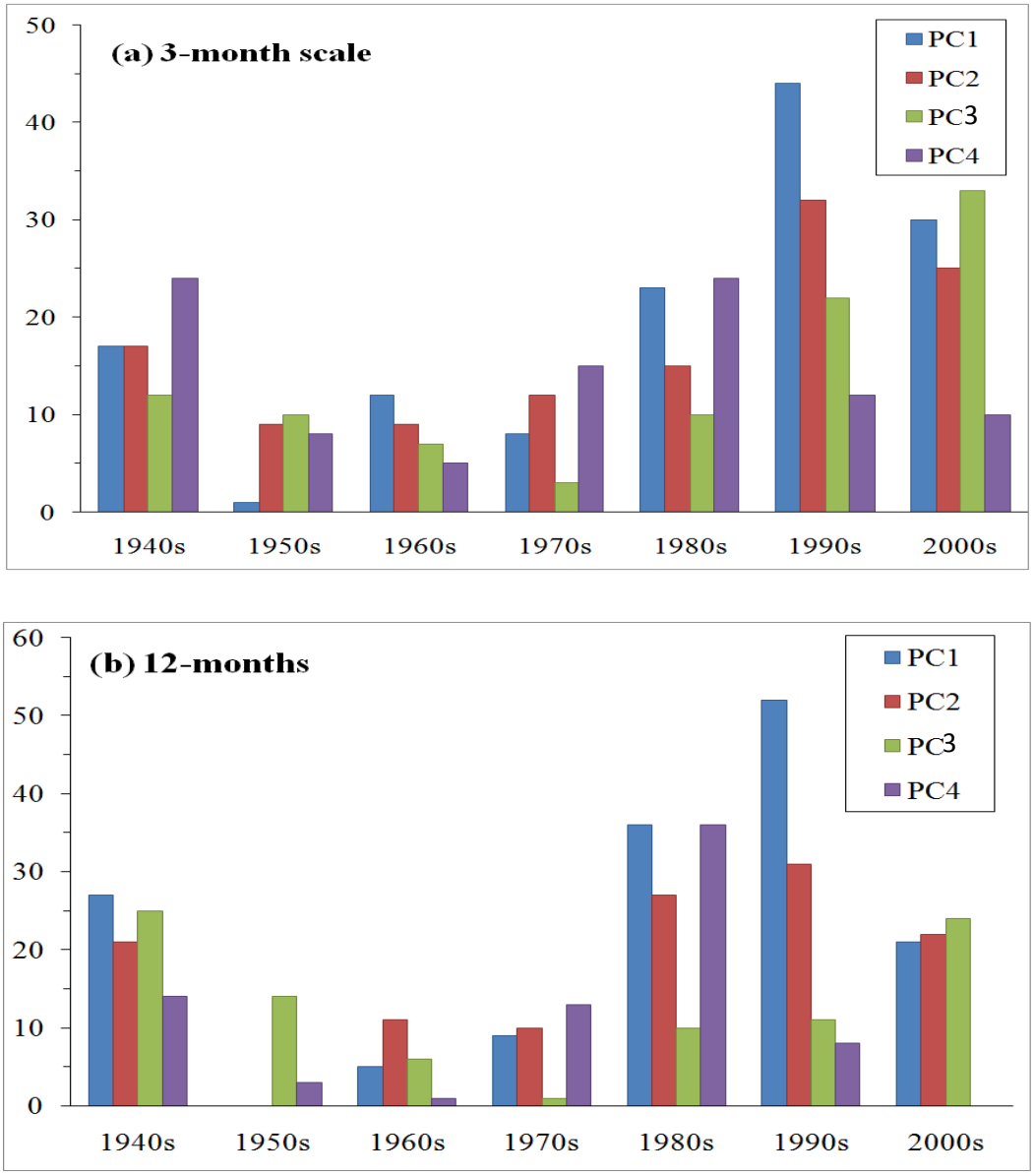

Figure 4: Histograms of the droughts frequency for the 3-month and 12-month SPEI for the four areas. The number of droughts is represented in blue, red, green and purple respectively for the 1st, 2nd, 3rd and 4th Areas, which correspond to the scores of PF1, PF2, PF3 and PF4 respectively.

At 3-month scale, the frequency of PF1 increases from one dry month per decade in the 1950s, nine in the 1970s, to 44 dry months per decade in the 1990s; PF2 from eight months per decade in the 1950s, 12 in the 1970s, to 32 months per decade in the 1990s; PF3 varies from 10 months per decade in the 1950s, three in the 1970s, to 22 months per decade in the

1990s; and PF4 from eight months per decade in the 1950s, 15 in the 1970s, to 12 months per decade in the 1990s. At 12-month time scale, the frequency of PF1 drought increases from no dry month in the 1950s, nine in the 1970s, to 50 dry months per decade in the 1990s; PF2 from no dry month in the 1950s, ten in the 1970s, to 31 dry months per decade in the 1990s; PF3 varies from 14 dry months in the 1950s, one in the 1970s, to 11 dry months per decade in the 1990s; and PF4 from three dry months in the 1950s, 13 in the 1970s, to eight dry months per decade in the 1990s. In general, we observe a gradual increase in drought frequency, especially since the 1970s, exception made of PF4 frequency. This is consistent with the 4th IPCC report (IPCC, 2007), which attributed the increase to global warming and projected that it may continue in the future.

Another interesting thing to notice is that the highest frequency of the drought patterns occurs during different decades: PF1 and PF2 in the 1990s; PF3 in the 2000s (also in the 1940s at 12-month scale); and PF4 in the 1980s (also in the 1940s at 3-month scale). However, all the drought patterns show the least frequency within the 1950s and the 1970s.

The figure shows that the decade of the 1990s was the driest decade for areas one and two since they both experienced more than 25% of all dry events that occurred between 1940 and 2009 in the 1990s, 1980s was the driest for area four while the driest decade for are three was 1990s (1950s) considering the 3-month (12-month) SPEI. There is also a positive trend in the drought frequency at all-time scales and in all the most areas. Thus, the number of droughts has been gradually increasing since the 1970s over areas 1, 2 and 3. Results also show that they all experienced a drastic drop in the number of dry events at all time-scales in the 1950s, except for Area 3 which showed a serious decrease in drought frequency in the 1960s and no drought at all in the 1970s.

4.1.4 The wavelet structure of the drought patterns

Figure 5 shows the wavelet power spectra (WPS) of the 3-months scores' PFs and their corresponding global wavelet spectrum (GWS). It reveals the power variability of the different cycles that temporarily dominate the PFs over the years. Overall, the power is

mostly distributed in the band of the 2-8 year period in all PFs, with a significance level of 5%, for the whole interval of time considered. The cycle with periodicity of less than or equal to one year is probably a representation of the seasons, and it won't retain our attention in this study.

In PF1, the 2-4 year periodic band cycle presents a strong significant power for the intervals from mid-1965s-1975s and from mid-1990s onwards, while the 4-8 year periodic band cycle shows strong power from the mid-1950s to mid-1990s and the 8-16 year period from the late 1990s till mid-2000s. The same score has a very strong 1-2 year of periodicity cycle that was active in the late 1960s. At the same time, the corresponding global wavelet spectrum (GWS) in Fig 5a shows a higher variance in the 2-8 year periodicity band, which is in agreement with the WPS, though, on the other hand, the very low power over the 4-8 years band during the intervals 1955-1970 and 1975-1995 in the WPS does not manifest in the GWS. The first score's spectrum presents a dominant phenomenon, of around 25 years of period, which was active from the 1940s till the beginning of 1990s. There are also several weak processes that were active for shorter periods: one with 4-7 years of oscillations from the mid-1940s to the 1950s and the 1980s to the mid-2000s; the other with a period of 2-4 years that was active in the 1970s.

The cycle with the highest power in PF2 is the 4-8 years of periodicity cycle (Fig 5b); it shows the strongest power from the 1970s till the end of the period of study, with a slight increase in the period length. However, this cycle shows the highest power in the 1980s, a time when it was also significant, but, surprisingly, it does not manifest in the corresponding GWS. This might be owing to the lack of influence of the cycle before the 1970s. The 1-2 year periodic band cycle in PF2, presents a strong significant power in the late 1950s, late 1990s and mid-1980s, while the 2-4 year cycle shows strong power for the intervals mid-1940s to 1950 and in the 1980s. The score of PF2 shows a spectrum with many strong processes that have a period of 2-3 years during almost each decade, one with 4-7 years of oscillation active from the mid-1970s to the 1990s. However, we also identified a weaker process that was active in the 1970s and presented an oscillation period of about 16 years.

In PF3, the cycle of 1-2 years of period presents strong significant power over the intervals of mid-1970s - mid-1980s and mid-1990s till early 2000, while the 2-4 years of periodicity cycle shows significant strong power between 1960 and the mid-1970s. This PF also presents another cycle in the 4-8 years band that shows significant strong power during the interval mid-1940 to mid-1960s and 1980-1995. The 8-16 year periodic band cycle presents very weak non-significant power from 1960-1970 and in the 1990s, which is consistent with the corresponding GWS and which shows no peak for the periodicity of 8-16 years (Fig 5c).

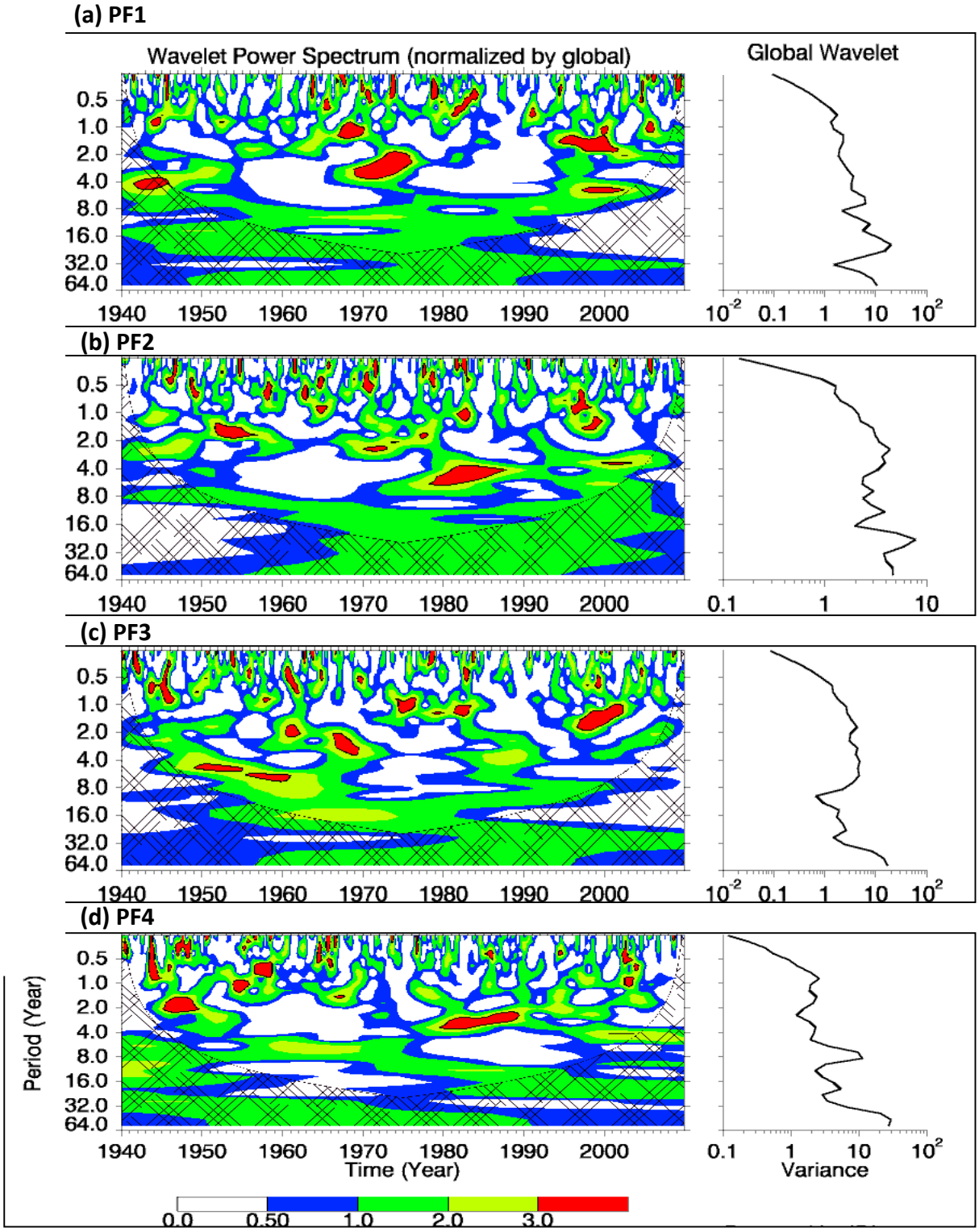

Figure 5: Wavelet power spectrum (using the Morlet wavelet) of scores of (a) PF1, (b) PF2, (c) PF3 and (d) PF4. Cross-hatched with line indicate the "cone-of-influence" (The cone of influence delimits the region of the wavelet power spectra where the edges effects become important). The black line contour is the 5% significant level.

For PF4, in addition to the 1-2 periodic band cycles that present very strong power from the 1940s-1960, in the end of the 1960s, 1970s, 1990s and in the early 2000s, there was another cycle in the 2-4 years of period band that also showed strong power from the mid-1940s to mid-1950 and from the end of the 1970s till 2000. Though this later cycle shows significant power during the interval from the end of the 1970s-1990, it does not reflect as a peak on the GWS, mostly because it was inactive in the 1960s - mid-1970s and in the 2000s. Moreover, PF4 wavelet spectrum shows 4-8 years of period cycle that had non-significant power from the mid-1950s to the mid-1970s, but which is reflected in the corresponding GWS (Fig 5d). DP4's spectrum shows only one strong signal of 7 years of period and that was active from the 1940s till the mid-1970s.

4.2 The influence of Atmospheric and Oceanic Tele-connections on the Southern African Droughts

Since it has been widely proven that droughts are linked to general global circulations, it is of interest to determine how droughts are influenced by the variation of the global SSTs. Here we are investigating the spatial relationship between the four principal modes that govern Southern African droughts with global SST over the four seasons followed by a temporal correlation between drought modes and different climate indices.

4.2.1 Sea Surface Temperature

Figure 6 shows correlations of the four scores with the SST at 3-months scale to quantify the relationship between the four PFs scores and global sea surface temperature.

At 3-months scale, PF1 shows strong negative correlations with equatorial Indian and Pacific oceans' SST during summer (DJF) and with equatorial Pacific Ocean SST and Atlantic Ocean SST (near Southern African coast) during Spring (SON). It also has weak correlation in some spot of the Pacific Ocean during MAM and JJA.

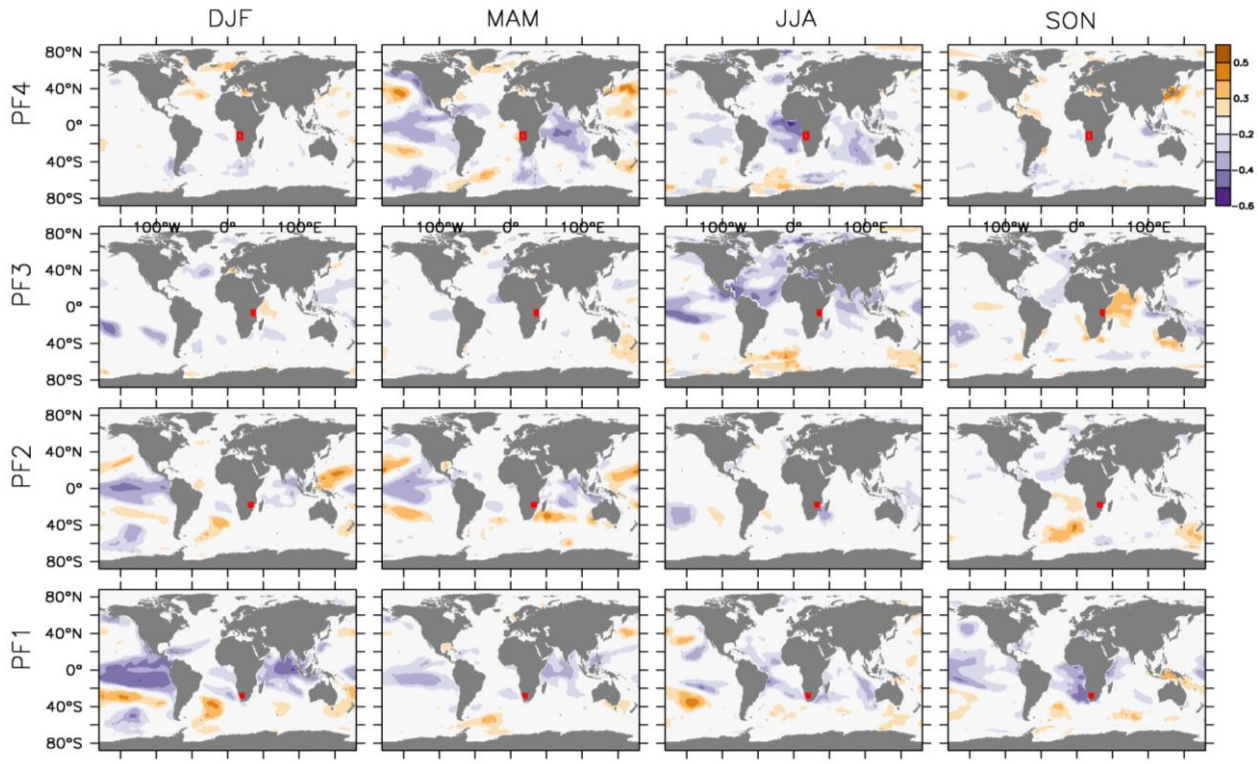

Figure 6: Correlation between SST and scores of PF1, PF2, PF3 and PF4 at different seasons.

PF2 presents negative correlation with the SST in the equatorial Pacific Ocean near America and positive near Japan. The negative correlation found by Manatsa et al. (2008) between Zimbabwe SPI and SST during SON season over the Pacific Ocean basin, the Indian and western Pacific oceans is not reflected in our results. This might be owing to the use of a different drought index and suggests that the SST over the Pacific Ocean basin, the Indian and western Pacific oceans have no influence on SON seasonal droughts in Zimbabwe, though they are strongly linked to the SON rainfall over the area.

It seems that PF3 does not have any relationship with the SST, except during winter, when it presents negative correlation with the North Pacific Ocean along the American and European coasts and the equatorial Atlantic. The fourth process shows weak correlation with the Indian and the eastern Pacific oceans during the winter and with the equatorial Atlantic

near West Africa during autumn. Correlation between the four scores with the SST at 12-months scale, are presented in Annexe 2. The PF1 shows a strong positive correlation with the Pacific and Indian oceans along the equator and the North Antarctic (near Alaska) during seasons DJF and MAM, and the Pacific, Atlantic and Indian oceans along the equator during the season SON. PF2 seems to have no relationship with global SST, except for very weak positive correlation in very small spots in the Pacific Ocean, while the third mode presents very weak positive correlation with the SST in the tropical Pacific Ocean, along the western coasts of the American continent and negative ones with the northern Pacific and Atlantic oceans. The fourth principal factor also presents a very weak link to SST in the middle of the equatorial Pacific.

4.2.2 Climate Indices

The wavelet coherence of each score with different climate indices is shown in Fig 7-10 respectively. These figures indicate the variability of their relationship over time. In general, the first principal factor shows stronger coherency with the SOI, IOD, TNA and the solar system indices. The SOI shows strong significance coherency with PF1 in the 2-8 year band which shift from an average period of seven years before 1960 to 2-4 years periodicity afterwards. The two also present strong coherence in the 1970s, over the 16-year and above band.

The most interesting thing to notice here is that though PF1 and the SOI index show mostly similar phases in the 1-2 years band and in the 2-4 years band, Fig 7 indicates that they experienced a shift in their phase in 1960, in 1980 and in 1990, changing from PF1 leading by 180 degrees to SOI leading by 90 degrees, a chaotic period and SOI leading by 90 degrees at each time respectively. The coherency of PF1 with the TNA index also shows a strong significant relation over the similar period band (2-4) as SOI, from the mid-1960s to the end of the 1990s, with a small interruption around 1980. TNA coherency with PF1 show a consistent phase: TNA leads by 90 degrees.

The IOD presents significant coherence with PF1 over the 8-16 years of period band, continuous from the mid-1950s to the 1980s and over the 1-2 years band from the mid-1940s till the mid-1950s and around the mid-1995. The IOD leads PF1 by 90 degrees over the 8-16 years band while PF1 always leads over the 1-2 years band with various degrees ranging from 45 to 90. The wavelet coherence spectrum between PF1 and TSA shows a strong relationship between them with a consistent phase of 90 degrees TSA leading, from 1960 till the mid-1990s over the 8-16 years band and in the 1990s over the 1-2 years band.

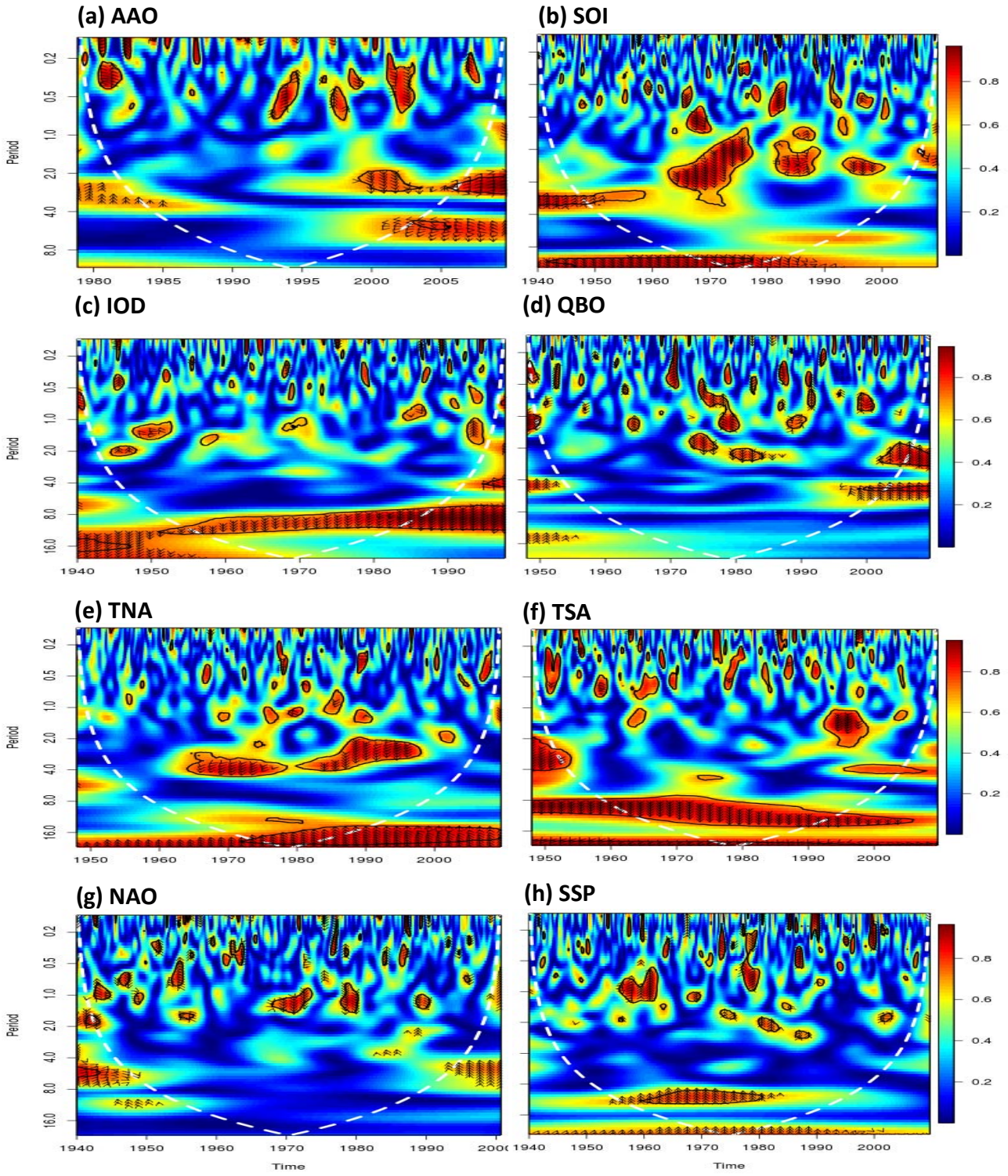

Figure 7: The wavelet coherence and phase of PF1 score with (a) AAO, (b) SOI, (c) IOD, (d) QBO, (e) TNA, (f) TSA, (g) NAO and (h) SSP indices. Dashed white line show the "cone-of-influence". The thick black line contour is the 5% significant level. Black arrows show the phase.

PF2 wavelet coherency spectra indicate that, since 1940 till the end of the 2000s, it has mostly been influenced by the IOD, NAO, TNA, TSA and SOI (Fig 8). Contrary to PF1 though, the score of PF2 shows a constant phase with the SOI index, where the latter always leads by 90 degrees. There is an exception though over the 4-8 years band in the 2000s, where the two present a non-significant coherence and PF2 leads SOI by 90 degrees. However, they have a strong coherence with each other over the 1-4 years band in the mid-1940s, in 1970 and in the 1990s, and over the 8-16 years band from the 1970s to the 1990s. The IOD presents strong coherency with the PF around the mid-1940s, from the early 1960s till the mid-1970s and early 1980s over the 1-4 years of period band, and from the mid-1950s to 1970 over the 8-16 period band. This result is consistent with Manatsa et al. (2012) who found that 1961 was a turning point in the Indian Ocean climate variability. In general, PF2 leads the IOD by 90 degrees over the 1-4 years of periodicity band, except from the early 1980s when they experienced a shift and the IOD led PF1 by 90 degrees, similar to their phase over the 8-16 years band.

PF2 also presents strong significant coherency with TSA over the 8-16 period band, continuous from the end of the 1960s till mid-1990s, where TSA leads by 90 degrees. They also present strong coherency over the 1-2 years band from the mid-1970s till the 2000s, with several interruptions like in early 1980s, mid-1980s, mid-1990s and early 2000.

Another climate index that shows high coherence with PF2 is TNA. These two present a strong relationship in the 1950s till early 1960s over the 2-4 years of period band and from the mid-1980s to the mid-2000s over the 4-8 years band. Though the 2-4 years of periodicity band show a consistency of phase, where TNA leads PF2 by 90 degrees, the 4-8 years band indicates continuous changes in their phase. The NAO and PF2 have strong significant coherence in the early 1950s, mid-1970s and early 1980s over the 1-2 years of periodicity band and from 1960 till the early 1970s, over the 2-4 years band. Their coherence phase shows that PF2 mainly leads with 90 degrees, with the exception of the 1970s, where NAO leads PF2 by 90 degrees over the 1-2 years band.

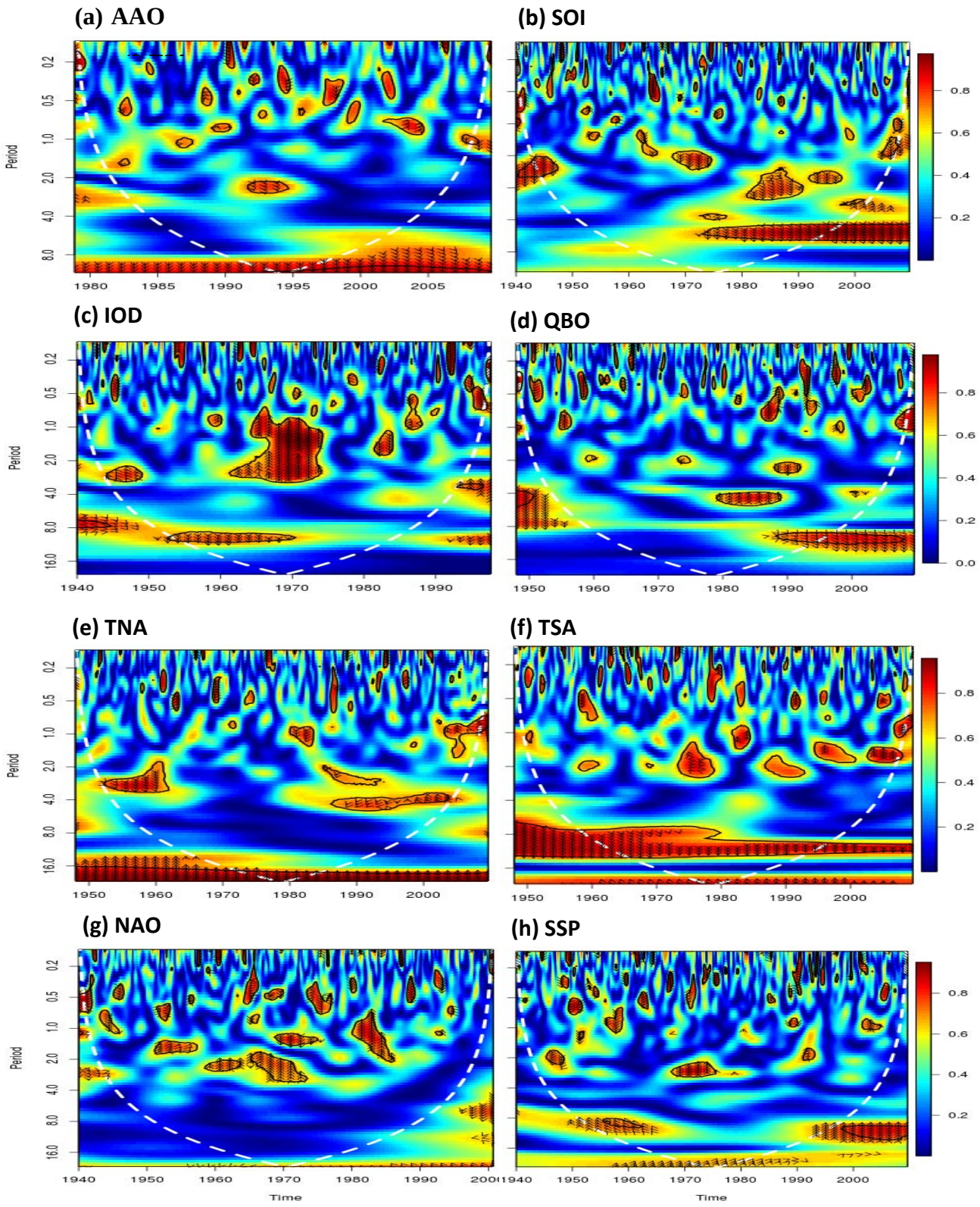

Figure 8: Same as Fig 7 but for PF2 score.

PF3 is mostly linked to the IOD, NAO, SOI and TNA (Fig 9). The strongest and continuous coherency is found between PF3 and TNA index over the 2-8 years of period band during the interval 1960s-early 1990s and around the mid-1970s over the 1-2 years band. The two show a consistent phase where TNA leads by 90 degrees. Exception is made for the period around the mid-1970s, when there are various phases. The SOI and PF3 indicate strong significant coherence mainly distributed in two bands: the 1-2 and the 2-8 years of period bands. In the 1-2 years band, the strongest coherences are located in the 1950s with PF3 leading by 90 degrees, while they are from the mid-1950s to early 1990s for the 2-8 years band with the SOI leading by 90 degrees. The strongest coherency between the IOD and PF3 lies in the 1-2 years of period band, from the early 1960s until the mid-1980s, with a gap around 1980, early 1980s and early 1990s. A lower coherence is found over the 4-8 years of period in the 1960s and a strong, significant one around the 1960s over the 2-4 years band. The IOD mostly leads PF3 by 90 degrees, except from the early 1990s over the 1-2 years of period where they experienced a shift of phase.

The relationship between NAO and PF3 is mainly located in the time interval between 1950 and 1990, over three different bands of period: from 1950 till the mid-1950s, early 1960s until the mid-1970s and early 1980s for the 1-2 years band; in the 1960s for the 2-4 years band and from the mid-1950s to the end of 1960s for the 4-8 years band. This confirms previous studies such as McHugh and Rogers (2001) that found negative correlation between summer rainfall station data over Tanzania and the NAO index. Though they keep a consistent phase with NAO leading PF3 by 90 degrees, they experience a change of shift after the mid-1970s and PF3 now leads by 90 degrees.

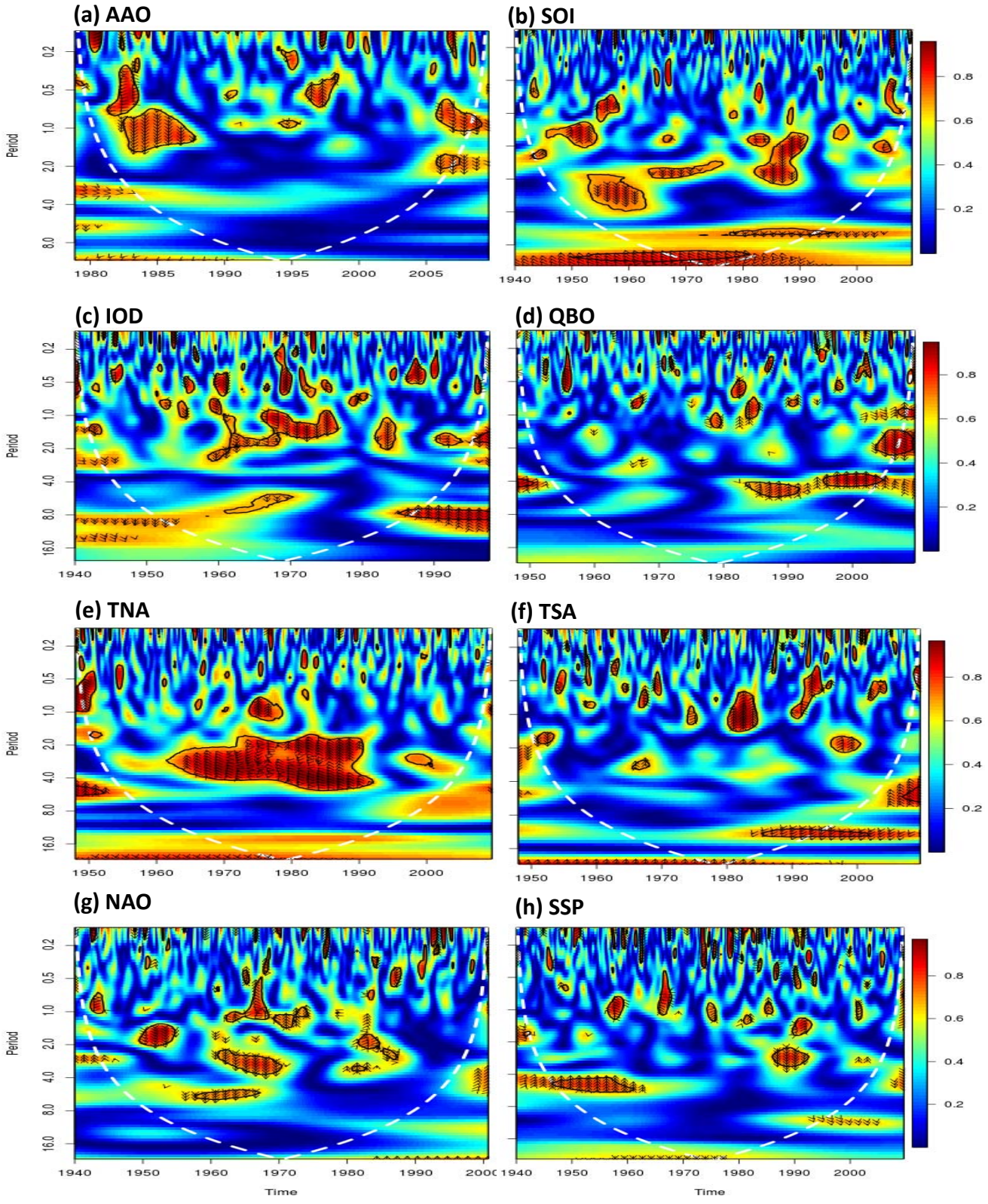

Figure 9: Same as Fig 7 but for PF3 score.

PF4 is the one that shows the poorest coherence with all climate indices, especially with the SOI, TNA and IOD, that showed strong coherence with the three other PFs. The strongest and significant coherence between PF4 and SOI is in the early 2000s, over the 4-8 years band. Everywhere else, they present weak coherence and for very short temporal expansion (terms of 1-2 years max.). The wavelet coherence spectrum of PF4 with IOD indicates strong coherence only as small spots in the early 1970s and early 1990s over the 1-2 years band of periodicity, while the one with TNA indicates significant coherence over the 1-2 years of period band as spots in the late 1970s, and over the 4-8 years band in the 1990s. These results indicate that these climate indices have little influence on PF4, and that there are other processes involved in defining this drought mode. However, TSA shows a continuous strong coherence with PF2 from the mid-1960s till mid-1990s (with PF4 leading by 90 degrees), over the 8-16 years band, and in the 1950s and 2000s (TSA leading by 90 degrees) over the 1-2 years band.

4.3 Summary

Figures 7 – 10 show that the climate indices that shows the highest correlation with drought in Southern Africa are SOI, IOD, TNA, TSA, SSP and AAO; but the persistence of those correlation varies among the drought patterns. Although, SOI influences all the drought patterns, its most persistent influence is on PF2, with a significant coherence at 8-16 year band in 1970-2009. IOD shows its most persistent influence on PF1, with a significant coherence at 8-16 year band in 1940-2009. TNA shows its most consistent influence on PF3, with significant coherence at 2-4 year band in 1960-1990. TSA shows a continuous influence on three drought patterns (PF1, PF2 and PF4), having a significant coherence with them at 8-16 year band in 1950-2009. SSP features its most persistent coherence with PF1 and PF3 at 8-16 year band (in 1950-1985) and 4-8 year band (in 1940-1960), respectively. AAO shows its most persistent significant coherence with PF1 and PF4 at 2-4 year band (1995-2009) and at 1-2 year band (in 1985-1995), respectively.

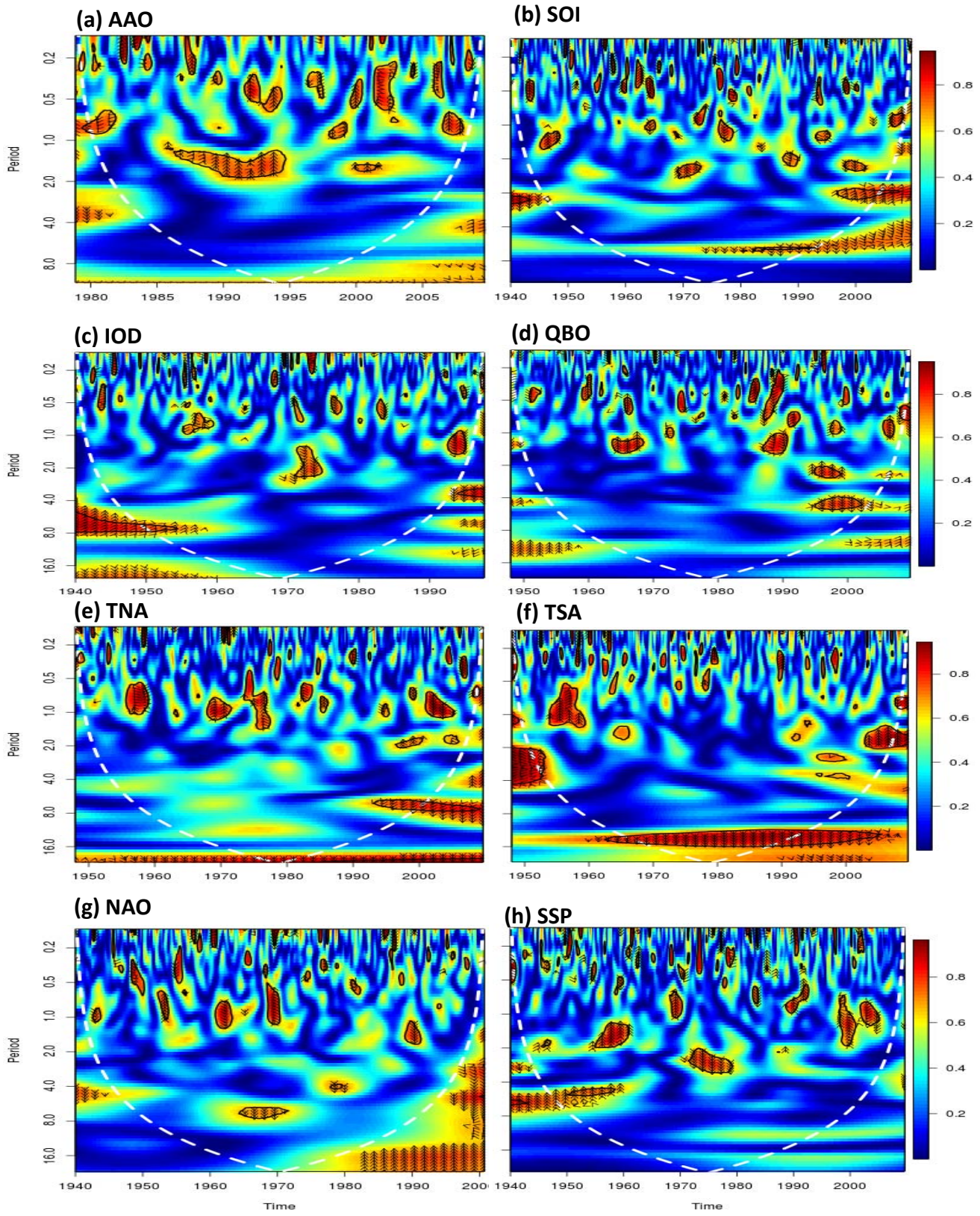

Figure 10: Same as Fig 7 but for PF4 score

Chapter V: The Characteristics of the Simulated Droughts over Southern Africa

In this chapter we evaluate how well climate models replicate past and present Southern African droughts. This is necessary to build our confidence in future drought projections simulated by the models. We first evaluated global climate models in the first section, downscaled regional climate models in the second, followed by a discussion on comparing RCMs' and GCM's abilities in capturing Southern African drought in the third part.

5.1 The GCM simulated Droughts

Figures 11 and 12 compare PCA loadings of the SPEI simulated from GCMs with those of the observed, at 3-month and 12-month respectively. Despite the shorter period spanned by the data, the PCA indicates drought patterns similar to the previous analysis on Southern African drought characteristics (1956-2002 and 1940-2009, respectively).

At the 3-month scale, CanESM2 performs better in reproducing the four drought modes (r=0.9 for all PFs). All models show a high ability in capturing the spatial pattern of PF1 and PF2 with a high correlation (r > 0.7; all models in PF1 and BCC-CSM, BNUESM, CNRMCM, FGOALS and MIROCESMCH in PF2). Most of the models simulated PF3 with a high correlation (r>0.7), but BCC-CSM and BNUESM show the lowest performance (r = 0.7 and 0.6, respectively), though they captured the spatial drought patterns. Furthermore, most models show their lowest performance in simulating the fourth drought pattern, PF4, with CNRM, GFDL2G and HadGEM2 indicating the lowest correlations (r = 0.3, 0.4 and 0.5 in that order). This might be owing to the fact that these three models present PF4's strongest loadings near the western equatorial region, while they are located in the western tropical region of sub-Saharan Africa in observed loadings. Another reason could be due to the definition of PF4 itself, as it needs to be orthogonal to the previous PFs (PF1-PF3).

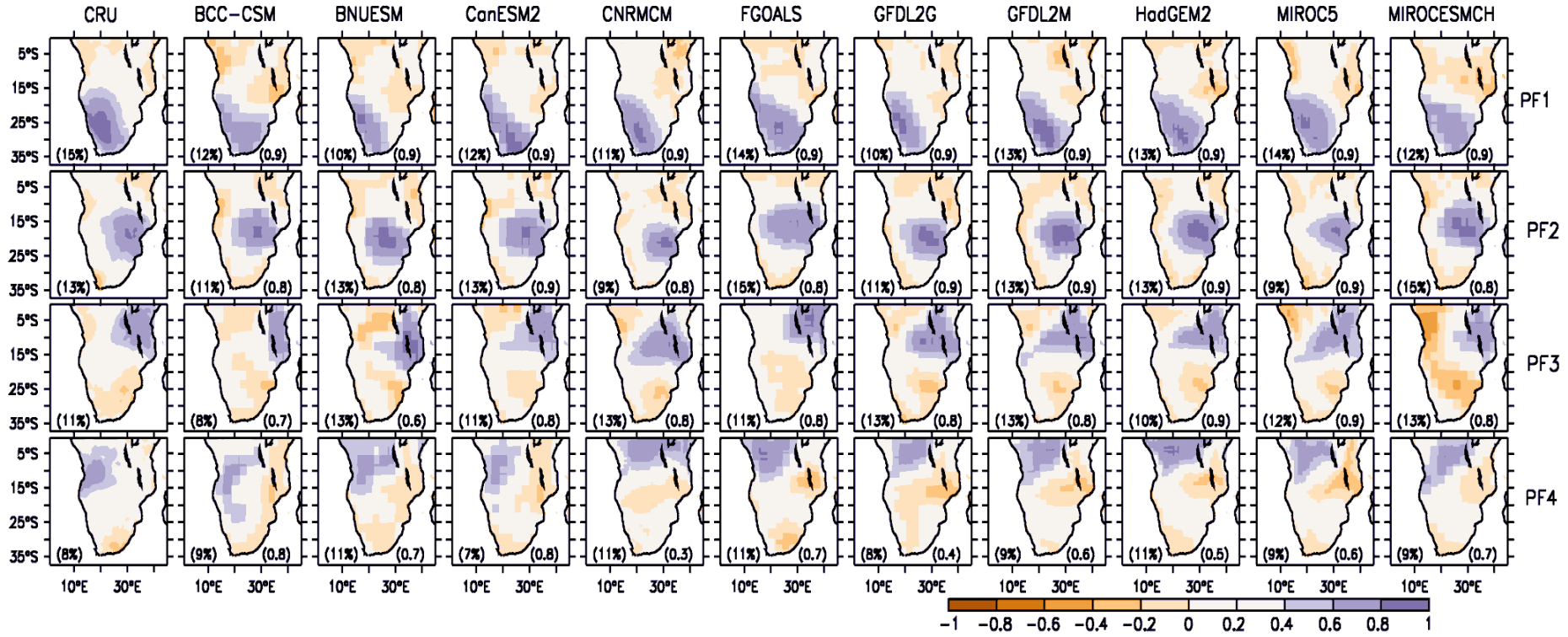

Figure 11: The observed and simulated PCA loadings of 3-m SPEI over Southern Africa by GCMs. The percentage of variance explained by each principal factor (PF) is indicated at the lower left corner of each panel. The spatial correlation between observed and simulated loadings for each model is shown at the lower right corner of the model's panel.

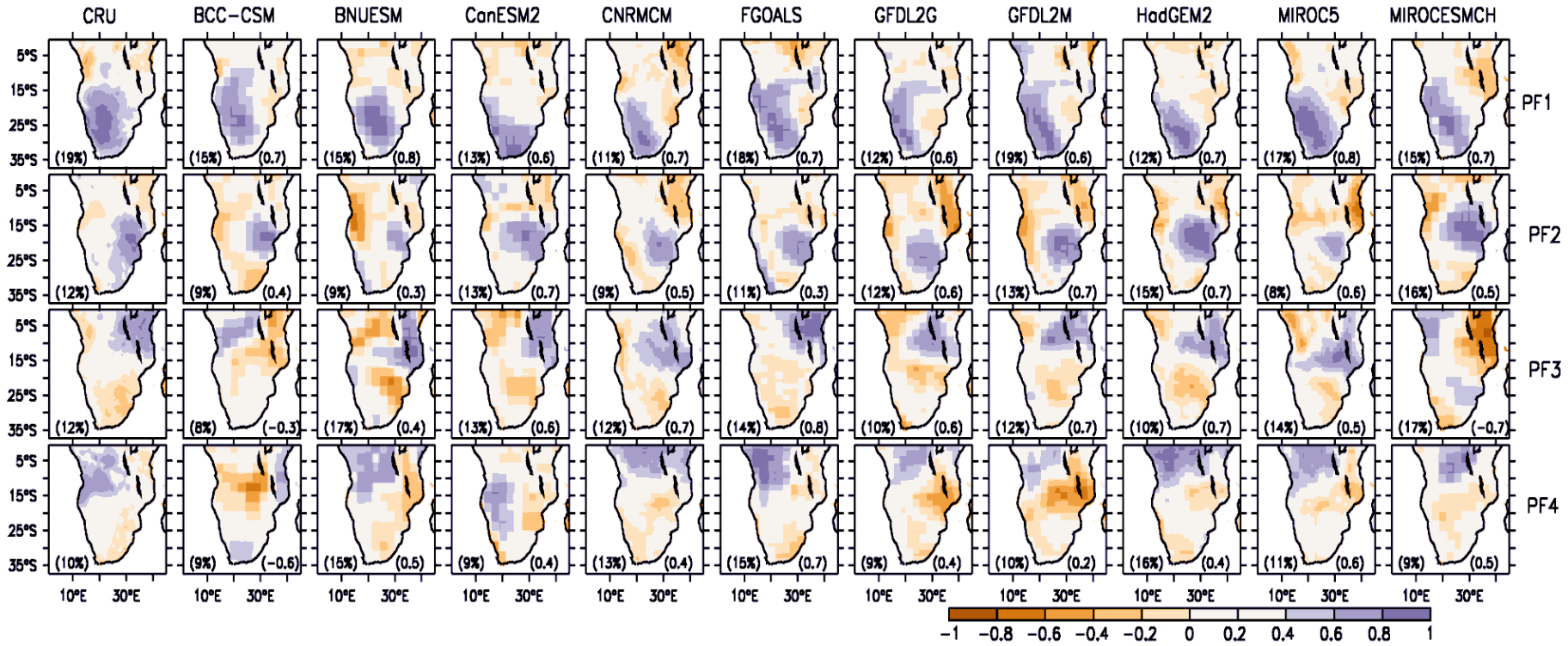

Figure 12: Same as Fig 11 but for the 12-month SPEI

As for the PF1 loadings at 3-months, but with a lower performance, all models captured spatial patterns of the 12-month scale PF1 (0.5 < r <0.9). In simulating this drought mode, BNUESM and MIROC5 indicate the highest correlation with observed loadings (r = 0.8), while CanESM2, GFDL2G and GFDL2M show the lowest performance (r = 0.6). Surprisingly, though it showed the highest correlation with PF1, BNUESM shows the lowest correlation (r = 0.3), similarly to FGOALS, with observed PF2, while CanESM2, GFDL2G and HadGEM3 present the best performance (r = 0.7). Three models did not capture well patterns of PF3: BCC-CSM, BNUESM and MIROC5 (r = 0.3, 0.4 and 0.5 respectively), while FGOALS presented the best performance (r = 0.8). Most of the models poorly reproduce PF4 loadings (the least performing model is GFDL2M; r = 0.2), with the exception of FGOALS, BCC-CSM and MIROC5, which present a quite good correlation with observed loadings (r = 0.7, 0.6 and 0.6 respectively).

Results show that, in general, all models are performing better at 3-month scale than at 12-month scale; 70 % of the models simulate well all four drought patterns (r > 0.5) at 3-month scale, while only 60% capture at least three of the drought patterns at 12-month scale (r > 0.5). A close inspection of Figures 11 and 12 reveals that some models present patterns that are significantly different to those of the observed. The reason might be owing to the possibility that some of the first four observed principal factors might be simulated with such a low variance so that they are not ranked among the first four for a particular model. In this case, they would not appear in our results, and another different pattern, not present in observed drought patterns, would have been used.

5.2 The RCM simulated Droughts

5.2.1 Spatial patterns

Figures 13 and 14 show the spatial drought patterns of RCMs and observations at 3 and 12-month scales, respectively. An important point to notice is that the four modes obtained in this

case differ from those obtained previously in subsection 5.1. In fact, the period of availability of RCM data was much shorter (1989-2007) than for the GCM (1956-2002). Hence, in order to accommodate the required dimensions for the PCA (time-number of grid cells), we had to reduce the area of the region of study (fewer grid cells). As a result, the drought pattern named PF3 in our previous discussions, whose strongest features are over Tanzania, has been replaced by a new drought pattern. In general, all models performed better at 3-month than at 12-month scale.

At 3-month scale, only few RCMs showed a very high correlation (r=0.9) with any observed pattern, except for REGCM3 for PF1 and RACMO2 for PF3. All models simulated well the first three patterns, despite some slight differences in their performance. For PF1, the correlation with the observed range stretched from 0.6 to 0.9 for all RCMs, with RCA35, REMO and WRF3 showing the least performance (r=0.6). The performance of the models in capturing spatial patterns of PF2 and PF3 is quite good; all models show a correlation with observations ranging from 0.7 to 0.8 for PF2 and from 0.7 to 0.9 for PF3. For both PF2 and PF3, four models exactly show a high correlation of r=0.8 with observed loadings, while the rest have a lower but still strong, correlation (0.7); these are CCLM, RACMO2, REGCM3 and REMO for PF2 and CCLM, CNRM, CRCM5 and REMO for PF3. The last drought pattern, PF4, is the one most models struggled most to simulate, the least performing being CNRM and RACMO2 (r=0.5), while the best simulations were obtained from CCLM, REGCM3, REMO and WRF3, though they also do not feature a very high correlation (r=0.7).

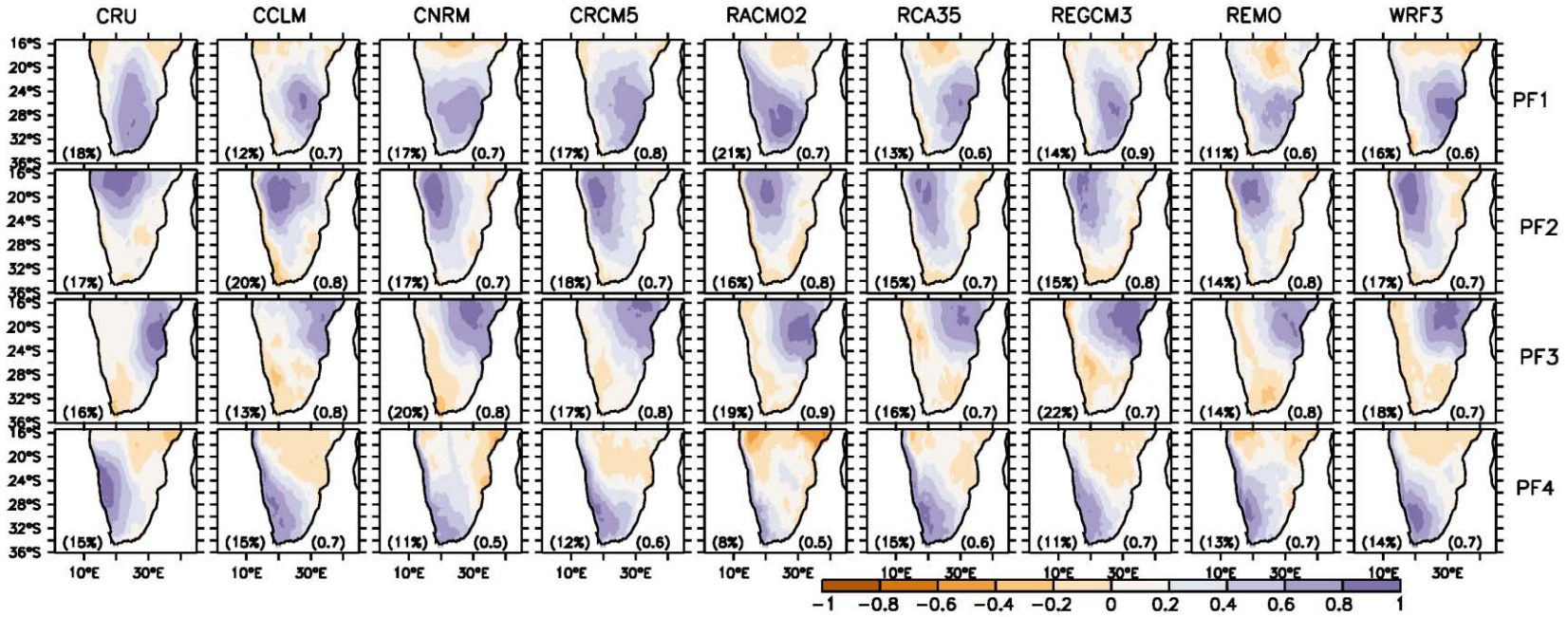

Figure 13: The observed and simulated PCA loadings of 3-month SPEI over Southern Africa by RCMs. The percentage of variance explained by each principal factor (PF) is indicated at the lower left corner of each panel. The spatial correlation between observed and simulated loadings for each model is shown at the lower right corner of the model's panel.

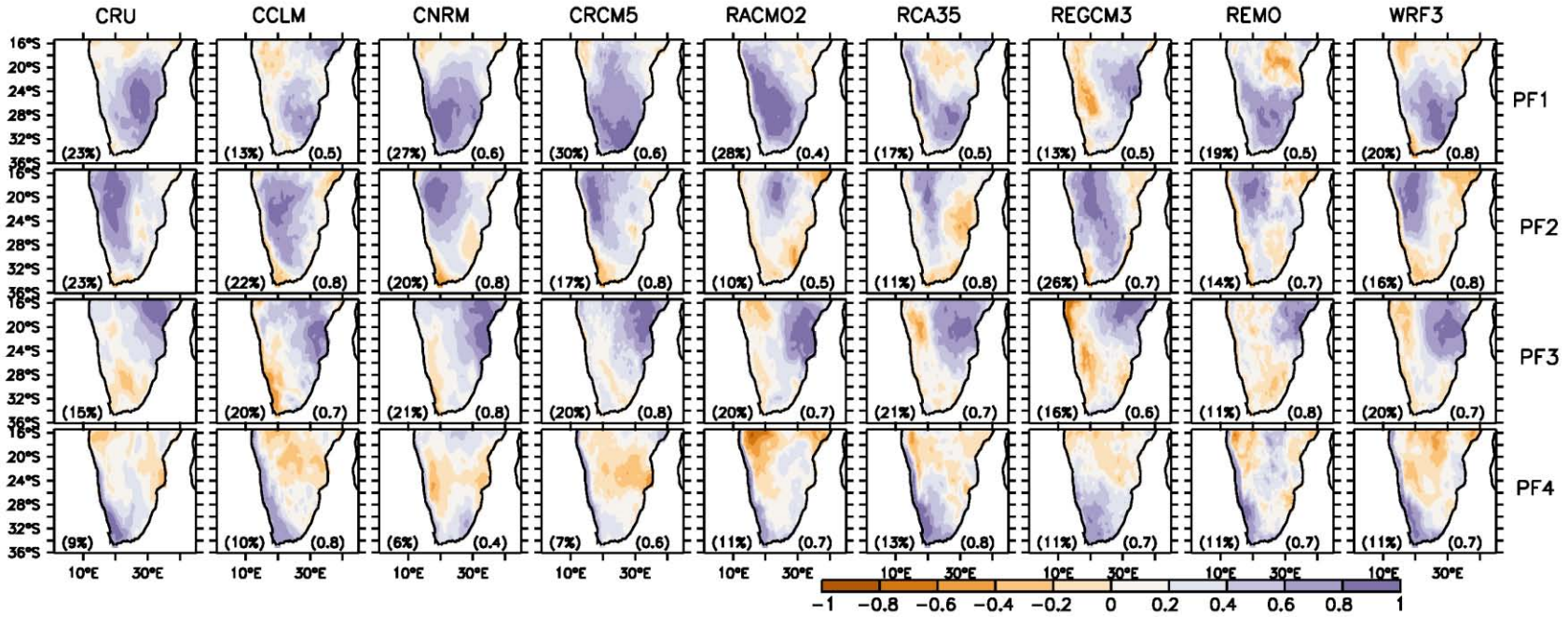

Figure 14: Same as Fig 13 but for 12-month SPEI.

The performance of the models in simulating all PFs at 12-month scale is, in general, not as good as for the 3-month scale. The range of the correlation of simulated and observed drought patterns contains lower values than the one obtained at 3-month scale for all PFs. For PF1, only three models captured spatial patterns of the drought mode (r>0.5). WRF3 performed better (r=0.8), followed by CNRM and CRCM5 (r=0.6), while RACMO2 indicates the lowest performance with a correlation of r=0.4. Furthermore, RACMO2 is the only model that does not capture spatial patterns of PF2 (r=0.5), while all other models indicate high correlations with observed loadings (r=0.8 and 0.7). In addition, all models simulated well PF3 loadings, with REGCM3 showing the least correlation with the observed (r=0.6), and CNRM, CRCM5 and REMO the highest (r=0.8). All models captured the spatial drought pattern PF4 except CNRM (r=0.4), with CCLM and RCA35 showing the best performance (r=0.8).

Similarly to GCMs, results indicate that all RCMs also perform better at 3-month scale than at 12-month scale. An analysis of Figures 13 and 14 reveals that 75 % of the models simulate well all four drought patterns (r > 0.5) at 3-month scale, while only 25% of them perform well in simulating at least three drought patterns at 12-month scale. It is quite interesting to note that none of RCMs has been able to reproduce patterns of all the four Southern African drought modes at 12-month scale. From the above results, one can conclude that RCMs simulate better observed patterns of short-term droughts' modes than long-term ones.

5.2.2 Temporal variations

Figures 15 and 16 show the seasonal correlation of observed and simulated scores of all PFs at both 3 and 12-month scale, respectively. In both figures, correlations are plotted versus normalized standard deviation; the normalized standard deviation is obtained by dividing the standard deviation of simulated score by the observed one. The vertical and the horizontal lines represent the normalized standard deviation (nst), while the top curve shows the variation of the correlation.

At 12-month scale, all models captured very well the variability of all the drought patterns during all seasons (normalized standard deviation is almost 1). In general, the temporal variation was well simulated by most models for PF1, PF3 and PF4 ($r > 0.3$), but almost all models seem to struggle in simulation the temporal evolution of PF2 ($r < 0.4$), except two of them (CCLM and CNRM). In general the performance of each model varies with each PF and each season. The model CNRM seems to be a particular case, since, among all the other, it is the one that performs better in simulating the temporal variation of PF1 and PF2 ($r \sim 0.8$ and 0.7 respectively) for all seasons, except in simulating PF2 during winter, when it is outperformed by CCLM. Three models (RCA35, REGCM3 and REMO) poorly reproduce the temporal evolution of PF3 ($r<0.4$), while REGCM3 totally misses PF4 seasonal variability during MAM and JJA ($r<0.3$).

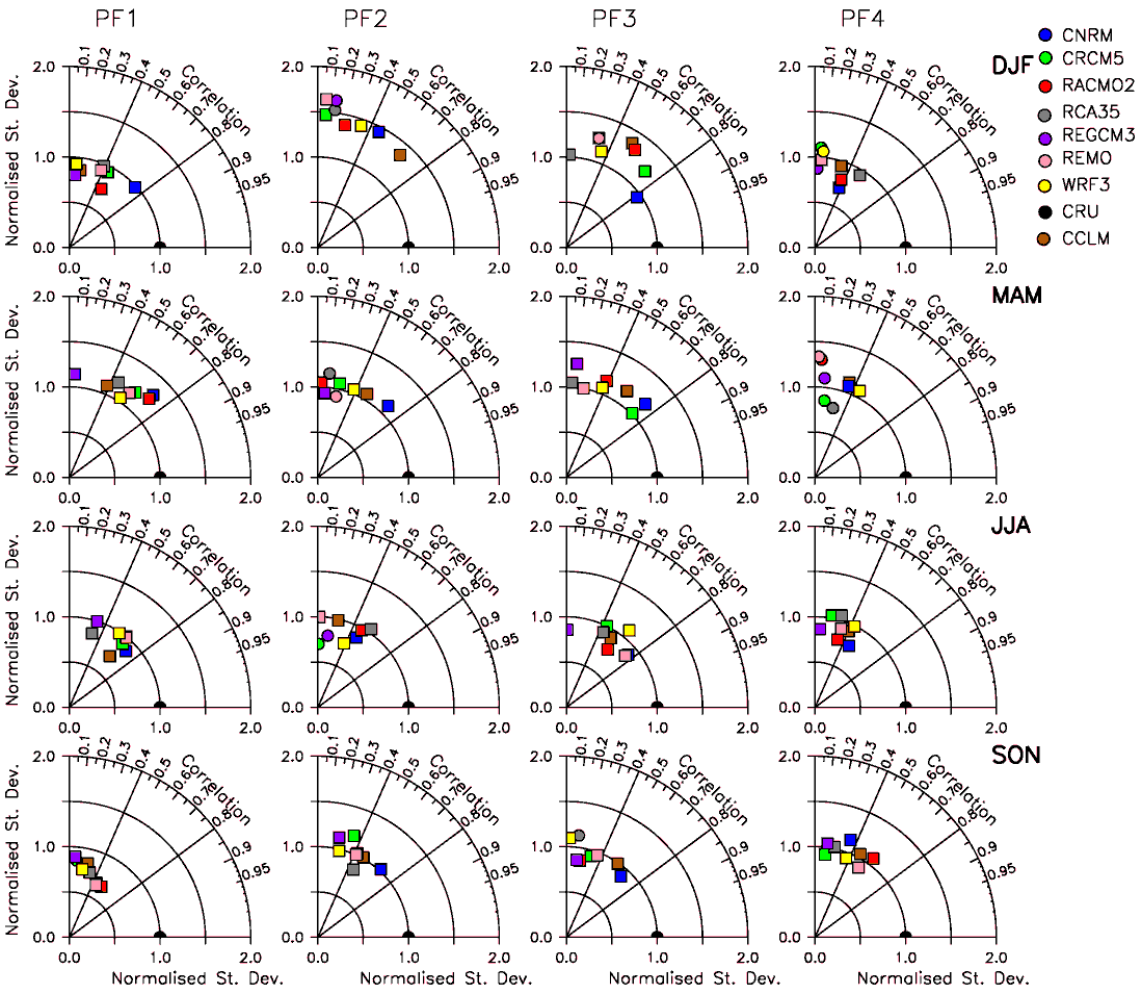

Figure 15: Taylor plots of the correlation between observed and simulated PCA scores (from RCMs driven by reanalysis) of 3-month SPEI over Southern Africa. Positive correlations are represented by the circles while the squares stand for negative correlations.

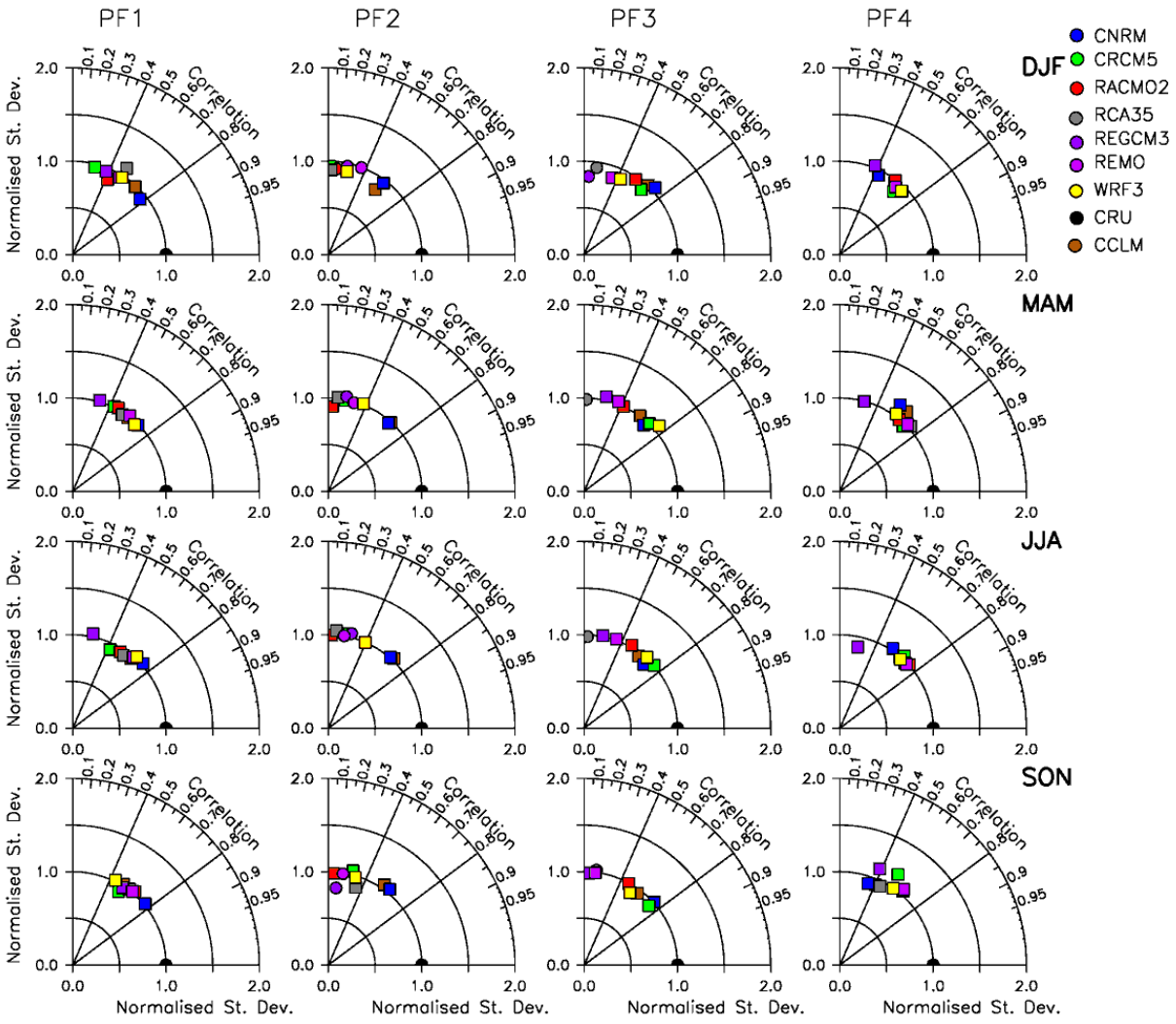

Figure 16: Same as Fig 15 but for the 12-month SPEI.

For 3-month scale, most models slightly over/underestimate the variability of the temporal pattern of the drought mode, especially for PF2, where all models overestimated the variability shown by observed score during summer (nst ~ 1.5). For PF1, most models indicate a better performance during MAM and JJA than during the other two seasons, except for model REGCM3 that failed to reproduce the drought mode evolution during MAM. Similarly to its simulation of the 12-month scale PF2, CNRM and CCLM perform well in simulation of the temporal evolution of PF2 at 3-month scale during most seasons, but show least performance during JJA. In general the performance of the temporal variability of the PF4 drought mode at 3-month scale is lower than that at 12-month scale ($r < 0.5$ for many).

5.3 Discussion

The consistency and stability of the four drought patterns obtained from observed data and GCMs simulations, independently of their different period of definitions, suggests that these modes are very robust. Furthermore, the fact that those that are still in the domain of definition of the RCMs simulation still appear, strengthens this assumption.

From the above results, one can conclude that GCMs reproduce better observed patterns of short-term droughts' modes than long-term droughts' ones. It is also quite interesting to note that all GCMs have been able to reproduce patterns of mode 1and2 entirely and mode 3 at 3-month time-scale. One may conclude that GCMs capture very well geographical patterns of Southern African drought's leading patterns, though they failed to simulate drought seasonal variations.

Another interesting fact is that RCMs capture better the temporal seasonal variability of observed score at 12-month scale than at 3-month scale, though performing better in simulating the 3-month scale spatial patterns of the drought mode than the 12-month loadings.

Chapter VI: Conclusion and Recommendation

In the paper, we have studied the spatial-temporal structures of Southern African droughts and examined the capability of the state-of-art global climate models in simulating the drought patterns. To account for the influence of both rainfall and temperature variability on the drought, we used SPEI to characterize the droughts. The SPEI was calculated at 3- and 12-month scales over the Southern African region, using monthly temperature and rainfall from CRU data (1940 – 2009) and GCMs simulations (1956-2009).

We used PCA on the SPEI to obtain the four dominant patterns over the region and used wavelet analysis to describe temporal variations of the drought and their coherence with various atmospheric tele-connections (depicted with climate indices). Finally, the study assessed the ability of 18 CMIP5 models (10 GCMs and 8 RCMs) to simulate Southern African droughts, especially their ability to capture the droughts' leading patterns over the region.

In general, all models have reproduced reasonably well the atmospheric general features that induce droughts in Southern Africa with 75 % of the RCMs and 70 % of the GCMs performing very well in simulating all four drought spatial patterns ($r > 0.5$) at 3-month scale.

A key question is to understand what causes the poor performance of models in reproducing long-term SA droughts. This might be owing to the fact that there are some processes that could influence drought but that are difficult to evaluate and, thus, might not be incorporated into the models (Sheffield and Wood, 2008), such as anthropogenic forcing (land use, irrigation and water diversion) and natural processes (vegetation dynamics and wildfire). Another reason might be the fact that the SPEI could be very sensitive to any low rainfall variability during dry season. Further research is needed to investigate the subject further.

The study also assessed the characteristics of SA droughts. Result have shown the existence of four principal drought modes, which explain conjointly more than 40% of the variance in

the SPEI, that have their strongest influence over the south-western part of Southern Africa (i.e. South Africa, Botswana and Namibia common border), Zimbabwe, Tanzania, and Angola, respectively. An increase in the drought intensity has been noticed, especially from the 1970s, at both 3- and 12-month scale. These results are in line with previous studies that suggested that there has been an increase in drought intensity and spatial expansion since the 1970s (Rouault and Richard, 2005; Manatsa et al., 2008; Lamb, 1996; Richard et al., 2001).

6.1 Summary

The results from the studies can be summarized as follows:

- About 50% variance in the SPEI over Southern Africa can be represented with four main drought patterns. The drought patterns (PF1, PF2, PF3 and PF4) feature their maximum variance over the south-western part of Southern Africa (i.e. South Africa, Botswana and Namibia common border), Zimbabwe, Tanzania, and Angola, respectively.
- The drought patterns have strong correlation with different ocean basins and the strength of the correlation varies with season. While PF1, PF2 and PF4 are strongly correlated with SST over the South Atlantic, Tropical Pacific and Indian oceans, PF3 is strongly correlated with the SST over the Tropical Pacific, Atlantic and Indian oceans.
- The drought patterns also have significant coherence with some climate indices, though the strength, duration, and phase of the coherence vary with time. However, the climate indices with most persistent influence on the drought patterns are SOI, IOD, TNA, TSA, SSP and AAO.
- The GCMs give remarkable representation of the drought patterns, but they perform better reproducing the drought patterns at 3-month scale than at 12-month scale. About 70% of the GCMs simulate all drought patterns well at 3-month scale, while only 60% of the GCMs simulate three of the drought patterns well at 12-month scale.

6.2 Recommendations for future studies

The results of the present study can be improved and applied in several ways. Firstly, the robustness of the drought pattern identified in this study can be improved by using more than one observation and reanalysis datasets, as there are significant differences among observational rainfall datasets. Secondly, the four drought patterns described in this study only account for about 50% of the SPEI variance in the datasets; meanwhile, the characteristics of the remaining 50% variance may be different from those described in the study. However, since the four drought patterns are the most significant patterns in the datasets, a good understanding and prediction of the temporal variability patterns may improve seasonal forecasting of drought in Southern Africa. A good understanding of how these drought patterns may change future climate under the influence of global warming may also reduce climate risks associated with drought occurrences in Southern Africa.

Moreover, the comparison between all used GCMs did require the regridding/interpolation to a common grid given that they were defined beforehand at different resolutions. This may have created a bias in the result caused by the method of regridding used (Joubert and Hewitson, 1997) and could explain the differences found between the results from GCMs and RCMs.

For future study, we recommend the investigation of Southern African drought projections using the SPEI. It might be interesting to use RCMs and GCMs projection to investigate the characteristics of future Southern African droughts. Also, whether the increase in drought characteristics, observed in Figs. 2-4, is owing to global warming or are part of a natural cycle should be investigated further. Furthermore, quantifying the relative role of temperature, precipitation and other climate variables on the SPEI variability would be an interesting topic for further studies.

6.3 Publications

One article based on results from the current study has been written and submitted for publication in an international journal “Climate Dynamics”. The paper submitted is entitled “Drought patterns in Southern Africa and how well GCMs simulate them”.

References

Abramowitz, M., & Stegun, I. A. (1965). *Handbook of Mathematical Functions* (1972nd ed., pp. 1–12).

Bergueria, S., & Vicente-Serrano, S. M. (2013). Calculation of the standardized Precipitation Evapotranspiration Index. doi:10.1175/2009JCLI2909.1.http

Blamey, R., & Reason, C. J. C. (2007). Relationships between Antarctic sea-ice and South African winter rainfall. *Climate Research*, *33*, 183–193.

Bradfield, L. (2009). Southern Africa Summer Drought and Heat Waves : Observations and Coupled Model Behavior. *Journal of Climate*, *22*, 6033–6046. doi:10.1175/2009JCLI3101.1

Burke, E. J., Brown, S. J., & Christidis, N. (2006). Modeling the Recent Evolution of Global Drought and Projections for the Twenty-First Century with the Hadley Centre Climate Model. *Journal of Hydrometeorology*, *7*(1990), 1113–1125.

Calow, R. C., Macdonald, A. M., Nicol, A. L., & Robins, N. S. (2010). Ground water security and drought in Africa: linking availability, access, and demand. *Ground water*, *48*(2), 246–56. doi:10.1111/j.1745-6584.2009.00558.x

Dai, Aiguo. (2011). Drought under global warming: a review. *Wiley Interdisciplinary Reviews: Climate Change*, *2*(1), 45–65. doi:10.1002/wcc.81

Dai, Aiguo, Trenberth, K. E., & Karl, T. R. (1998). Global Variations in Droughts and Wet Spells : *Geophysical Research Letters*, *25*(17), 3367–3370.

Dai, Aiguo;, Trenberth, E. K., & Qian, T. (2004). A Global Dataset of Palmer Drought Severity Index for 1870 – 2002 : Relationship with Soil Moisture and Effects of Surface Warming. *Journal of Hydrometeorology*, *5*, 1117–1130.

Farge, M. (1992). WAVELET TRANSFORMS AND THEIR APPLICATIONS TO TURBULENCE. *Annual Review Fluids Mechanics*, *24*(Holschneider 1991), 395–457.

Fauchereau, N., Trzaska, S., Rouault, M., & Richard, Y. (2003a). Rainfall Variability and Changes in Southern Africa during the 20th Century in the Global Warming Context, 139–154.

Fauchereau, N., Trzaska, S., Rouault, M., & Richard, Y. (2003b). Rainfall Variability and Changes in Southern Africa during the 20th Century in the Global Warming Context. *Natural Hazards*, 139–154.

Fitzgerald, D. L. (2005). Analysis of extreme rainfall using the log logistic distribution. *Environmental Research*, 249–257. doi:10.1007/s00477-004-0229-x

Giannini, A., Biasutti, M., Held, I. M., & Sobel, A. H. (2008). A global perspective on African climate. *Climatic change*, *90*, 359–383. doi:10.1007/s10584-008-9396-y

Giorgi, F. (2006). Climate change hot-spots, *33*(April), 1–4. doi:10.1029/2006GL025734

Gouhier, T. C., & Grinsted, A. (2013). Package " biwavelet ."

Haensler, A., Hagemann, S., & Jacob, D. (2011). The role of the simulation setup in a long-term high-resolution climate change projection for the southern African region. *Theor Appl. Climatology*, 106, 153–169. doi:10.1007/s00704-011-0420-1

Holm, J. D., & Morgan, R. G. (1985). Coping with Drought in Botswana : an African Success. *The Journal of Modern Studies*, *23*(3), 463–482. Retrieved from http://www.jstor.org/stable/160661

Hosking, J. R. M. (1990). L-moments: Ananlysis and Estimation of Distribution using Linear Combinations of Order Statistics. *Royal Statistical Society*, 105–124.

Ideião, S. M. A., & Santos, C. A. G. (2005). ANALYSIS OF PRECIPITATION TIME SERIES USING THE WAVELET TRANSFORM. *Sociedade & Natureza*, 736–745.

Jury, M. R., & Mwafulirwa, N. D. (2002). Climate variability in Malawi, part 1: dry summers, statistical associations and predictability. *International Journal of Climatology*, *22*(11), 1289–1302. doi:10.1002/joc.771

Jury, Mark R, & Enfield, D. B. (2002). Tropical monsoons around Africa : Stability of El Nin ˜ o – Southern Oscillation associations and links with continental climate, *Journal Geographycal Research*, *107*. doi:10.1029/2000JC000507

Jury, Mark R. (2002). Economic Impacts of Climate Variability in South Africa and Development of Resource Prediction Models. *Journal of Applied Meteorology*, *41*(1), 46–55. doi:10.1175/1520-0450(2002)041<0046:EIOCVI>2.0.CO;2

Jury, Mark R., Mulenga, H. M., & Mason, S. J. (1999). Exploratory Long-Range Models to Estimate Summer Climate Variability over Southern Africa. *Journal of Climate*, *12*, 1892–1899.

Labat, D. (2005). Recent advances in wavelet analyses : Part 1 . A review of concepts, *Journal of Hydrology*, *314*, 275–288. doi:10.1016/j.jhydrol.2005.04.003

Manatsa, D, Chingombe, W., Matsikwa, H., & Matarira, C. H. (2008). The superior influence of Darwin Sea level pressure anomalies over ENSO as a simple drought predictor for Southern Africa, *Theoratical Applied Climatology*, *92*, 1–14. doi:10.1007/s00704-007-0315-3

Manatsa, D., & Matarira, C. H. (2009). Changing dependence of Zimbabwean rainfall variability on ENSO and the Indian Ocean dipole/zonal mode. *Theoretical and Applied Climatology*, *98*(3-4), 375–396. doi:10.1007/s00704-009-0114-0

Manatsa, Desmond, Reason, C. J. C., & Mukwada, G. (2012). On the decoupling of the IODZM from southern Africa Summer rainfall variability. *International Journal of Climatology*, *32*(5), 727–746. doi:10.1002/joc.2306

Mason, S. J., & Jury, M. R. (1997). Climatic variability and change over southern Africa: a reflection on underlying processes. *Progress in Physical Geography*, *21*(1), 23–50. doi:10.1177/030913339702100103

Meehl, G. A., Stocker, T. F., Collins, W. D., Friedlinstein, P., Gaye, A. T., Gregory, J. M., … Zhao, Z.-C. (2007). Climate Change 2007: The Physical Science Basis. Contribution of Working Group I to the Fourth Assessment Report of the Intergovernmental panel on Climate Change. In S. Solomon, D. Quirion, M. Manning, Z. Chen, M. Marquis, K. . Averyt, … H. L. Miller (Eds.), *Global Climate Projections* (pp. 747–846). Cambridge University Press, Cambridge, united Kingdom and new York, NY, USA.

Mishra, A. K., & Singh, V. P. (2010). Review paper A review of drought concepts. *Journal of Hydrology*, *391*(1-2), 202–216. doi:10.1016/j.jhydrol.2010.07.012

Mitchell, T. D., & Jones, P. D. (2005). An improved method of constructing a database of monthly climate observations and associated high-resolution grids. *International Journal of Climatology*, *25*(6), 693–712. doi:10.1002/joc.1181

Nicholson, S. E., Leposo, D., & Grist, J. (2001). The Relationship between El Nino and Drought over Botswana. *Journal of Climate*, *14*, 323–335.

Nikulin, Grigory, and Coauthors, 2012: Precipitation Climatology in an Ensemble of CORDEX-Africa Regional Climate Simulations. J. Climate, 25, 6057–6078. doi: http://dx.doi.org/10.1175/JCLI-D-11-00375.1; URL: http://wcrp-cordex.ipsl.jussieu.fr/

Ntale, H. K., & Gan, T. Y. E. W. (2003). DROUGHT INDICES AND THEIR APPLICATION TO EAST AFRICA. *International Journal of Climatology*, *23*, 1335–1357. doi:10.1002/joc.931

Paavola, J. (2008). Livelihoods , vulnerability and adaptation to climate change in Morogoro , Tanzania, *Environmental Science & Policy, 11*, 642–654. doi:10.1016/j.envsci.2008.06.002

Palmer, C. W. (1965). *Meteorological Drought*. US Weather Bureau, Washington, D.C.

Potop, V., & Mozny, M. (2011). EXAMINATION OF THE EFFECT OF EVAPOTRANSPIRATION AS AN OUTPUT PARAMETER IN SPEI DROUGHT INDEX IN CENTRAL BOHEMIAN REGION. *Scientific Conference*, (September), 1–3. doi:10.1007/s00704-011-0460-6.Vicente-Serrano

Rao, S. a., Behera, S. K., Masumoto, Y., & Yamagata, T. (2002). Interannual subsurface variability in the tropical Indian Ocean with a special emphasis on the Indian Ocean Dipole. *Deep Sea Research Part II: Topical Studies in Oceanography*, *49*(7-8), 1549–1572. doi:10.1016/S0967-0645(01)00158-8

Ratna, S. B., Behera, S., Ratnam, J. V., Takahashi, K., & Yamagata, T. (2012). An index for tropical temperate troughs over southern Africa. *Climate Dynamics*. doi:10.1007/s00382-012-1540-8

Richard, Y., Fauchereau, N., Poccard, I., Rouault, M., & Trzaska, S. (2001). 20th century droughts in southern Africa: spatial and temporal variability, teleconnections with

oceanic and atmospheric conditions. *International Journal of Climatology*, *21*(7), 873–885. doi:10.1002/joc.656

Richard, Y., & Poccard, I. (1998). A statistical study of NDVI sensitivity to seasonal and interannual rainfall variations in Southern Africa. *International of Remote Sensing*, *19:15*, 2907–2920.

Rouault, M., & Richard, Y. (2003). Intensity and spatial extension of drought in South Africa at different time scales. *WaterSA*, *29*(4), 489–500.

Rouault, M., & Richard, Y. (2005). Intensity and spatial extent of droughts in southern Africa, *Geophysical Research Letters*, *32*(April), 2–5. doi:10.1029/2005GL022436

Saji, N. H., Goswami, B. ., Vinayachandran, P. N., & Yamagata, T. (1999). A dipole mode in the tropical Indian Ocean, *Nature, 401*(September), 360–363.

Sheffield, J., & Wood, E. F. (2008). Projected changes in drought occurrence under future global warming from multi-model, multi-scenario, IPCC AR4 simulations. *Climate Dynamics*, *31*(1), 79–105. doi:10.1007/s00382-007-0340-z

Shuttleworth, J. W. (1993). Evaporation. In H. McGraw (Ed.), *Handbook of Hydrology* (pp. 4.1–4.53).

Sivakumar, M. V. K. ., Motha, P. R., Wilhite, A. D., & Woods, A. D. (2011). *AgriculturAl Drought Indices. Proceedings of the WMO/UNISDR Expert Group Meeting on Agricultural Drought Indices*. *World Meteorological Organization*.

Taylor, K. E., Stouffer, R. J., & Meehl, G. a. (2012). An Overview of CMIP5 and the Experiment Design. *Bulletin of the American Meteorological Society*, *93*(4), 485–498. doi:10.1175/BAMS-D-11-00094.1; URL: http://cmip-pcmdi.llnl.gov/cmip5/

Thornthwaite, C. W. (1948). An Approach toward a Rational Classification of Climate. *American Journal Society*, *38*(1), 55–94. Retrieved from http://links.jstor.org/sici?sici=0016-7428(194801)38:1<55:AATARC>2.0.CO;2-O

Torrence, C., & Compo, G. P. (1998). A Practical Guide to Wavelet Analysis.

Torrence, C., & Webster, P. J. (1999). Interdecadal Changes in the ENSO – Monsoon System. *Journal of Climate*, *12*, 2679–2690.

Unganai, L. S., & Kogan, F. N. (1998). Drought Monitoring and Corn Yield Estimation in Southern Africa from AVHRR Data. *Remote Sensing Environment*, *4257*(63), 219–232.

USGS, T. U. W. S. S. (2013). Droughts: Questions and Answers. *U.S. Geological Survey*. Retrieved from http://ga.water.usgs.gov/edu/qadroughts.html

Vicenete-Serrano, S. M., López-Moreno, J. I., Gimeno, L., Nieto, R., Tejeda, E. M., Lacruz, J. L., … Molina, C. A. (2011). A multiscalar global evaluation of the impact of ENSO on droughts, *116*, 1–23. doi:10.1029/2011JD016039

Vicente-Serrano, S. M., Beguería, S., & López-Moreno, J. I. (2010). A Multiscalar Drought Index Sensitive to Global Warming : The Standardized Precipitation Evapotranspiration Index. *Journal of Climate*, *23*(7), 1696–1718. doi:10.1175/2009JCLI2909.1

Vicente-Serrano, S. M., Beguería, S., Lorenzo-Lacruz, J., Camarero, J. J., López-Moreno, J. I., Azorin-Molina, C., … Sanchez-Lorenzo, A. (2012). Performance of Drought Indices for Ecological, Agricultural, and Hydrological Applications. *Earth Interactions*, *16*(10), 1–27. doi:10.1175/2012EI000434.1

Vicente-Serrano, S. M., & López-Moreno, J. I. (2005). Hydrological response to different time scales of climatological drought : an evaluation of the Standardized Precipitation Index in a mountainous Mediterranean basin. *Hydrology and Earth System Sciences*, *9*, 523–533.

Vicente-Serrano, S. M., López-moreno, J. I., Drumond, A., Gimeno, L., Nieto, R., Morán-Tejeda, E., … Zabalza, J. (2011). Effects of warming processes on droughts and water resources in the NW Iberian Peninsula (1930 − 2006). *Climate Research*, *48*, 203–212. doi:10.3354/cr01002

Vicente-Serrano, S. M., Lopez-Moreno, J. I., Gimeno, L., Nieto, R., Moran-Tejeda, E., Lorenzo-Lacruz, J., … Azorin-Molina, C. (n.d.). A Multi-Scalar Global Evaluation of the Impact of ENSO on Droughts.

Villholth, K. G., Tøttrup, C., Stendel, M., & Maherry, A. (2013). Integrated mapping of groundwater drought risk in the Southern African Development Community (SADC) region, *Hydrogeology Journal, 21*, 863–885. doi:10.1007/s10040-013-0968-1

Vinayachandran, P. N., Francis, P. A., Rao, S. A., & Sciences, O. (2009). INDIAN OCEAN DIPOLE : PROCESSES AND IMPACTS. *Indian Academy of Sciences*.

Washington, R., & Downing, T. E. (1999). Seasonal Forecasting of AfFican Rainfall : Prediction , Responses and Household Food Security. *The Geographical Journal*, *165*(3), 255–274. Retrieved from http://www.jstor.org/stable/3060442

Washington, R., & Preston, A. (2006). Extreme wet years over southern Africa : Role of Indian Ocean sea surface temperatures, *Journal Geographycal Research, 111*, 1–15. doi:10.1029/2005JD006724

Wilhite, D. A., Svoboda, M. D., & Hayes, M. J. (2007). Understanding the complex impacts of drought : A key to enhancing drought mitigation and preparedness ∗. *Manage*, (15122), 763–774. doi:10.1007/s11269-006-9076-5

Annexe 1

Examples of three wavelet basis functions and their properties.

Function name	$\psi_0(\eta)$	$\psi_0(s\omega)$	**e-folding time** τ_s	**Fourier wavelength λ**
Morlet (ω_0) **frequency** =	$\pi^{1/4} e^{i\omega_0\eta} e^{\eta^2/2}$	$\pi^{\frac{1}{4}} H(\omega) e^{(s\omega\ \omega_0)^2/2}$	$\sqrt{2}s$	$\frac{4\pi\pi}{\omega_0 + \sqrt{2+\omega_0^2}}$
Paul **(m = order)**	$\frac{2^m i^m m!}{\sqrt{\pi(2\mathrm{m})!}} (1\mathrm{i}\eta)^{(m+1)}$	$\frac{2^m}{\sqrt{m(2\mathrm{m}\ \ 1)!}} H(\omega)(s\omega)^m e^{s\omega}$	$\mathrm{s}/\sqrt{2}$	$\frac{4\pi\mathrm{s}}{2\mathrm{m}+1}$
DOG **(m derivative)** =	$\frac{(\ 1)^{m+1}}{\sqrt{\Gamma\left(m+\frac{1}{2}\right)}} \frac{d^m}{d\eta\eta^m} \left(e^{\eta^2/2}\right.$	$\frac{i^m}{\sqrt{\Gamma\left(m+\frac{1}{2}\right)}} (s\omega)^m e^{(s\omega)^2/2}$	$\sqrt{2\mathrm{s}}$	$\frac{2\pi\pi}{\sqrt{m+\frac{1}{2}}}$

H(ω) = Heaviside step function, H(ω) = 1 if ω > 0, H(ω) = 0 otherwise.

DOG = derivative of Gaussian; m=2 is the Marr or Mexican hat wavelet.

Annexe 2

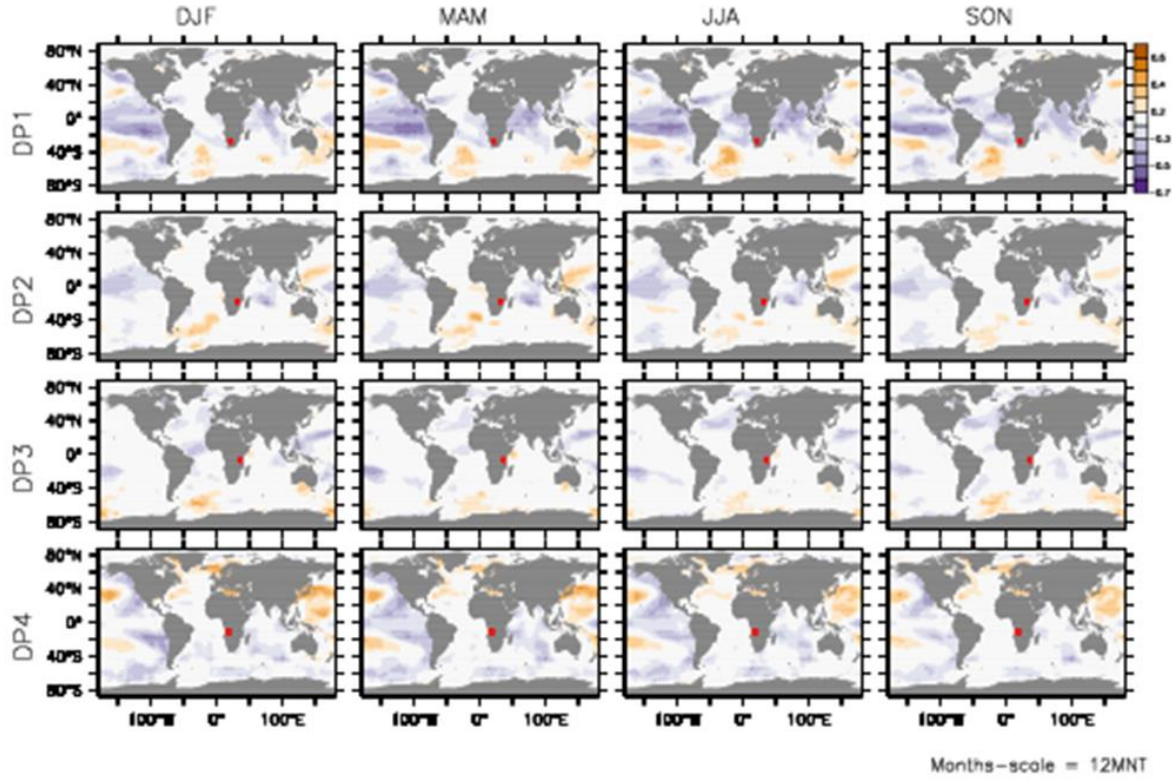

Figure 17: Correlation between SST and scores of PF1, PF2, PF3 and PF4 (here named DP1, DP2, DP3 and DP4 respectively) at different seasons.